Turbulent scalar fluxes from a Generalized Langevin model: implications on mean scalar mixing and tracer particle dispersion

Bertrand Naud[1, a)] and Dirk Roekaerts[2, 3]
[1)] *Modeling and Numerical Simulation Group, Energy Department, Ciemat, Avda. Complutense 40, 28040 Madrid, Spain*
[2)] *Department of Process and Energy, Delft University of Technology, Leeghwaterstraat 39, Delft 2628, CB, The Netherlands*
[3)] *Department of Mechanical Engineering, Eindhoven University of Technology, PO Box 513, Eindhoven 5600, MB, The Netherlands*

(Dated: 9 January 2021)

A Generalized Langevin Model (GLM) formulation to be used in transported joint velocity-scalar probability density function (PDF) methods is recalled in order to imply a turbulent scalar-flux model where the pressure-scrambling term is in correspondence with the standard Monin's return-to-isotropy term. The proposed non-constant C_0 formulation is extended to seen-velocity models for particle dispersion modeling in dispersed two-phase flows. This allows to correct the wrong turbulent scalar-flux modeling in the limit of tracer particles. Moreover, this allows to have a more general formulation in order to consider advanced Reynolds-stress models. The cubic model of Fu, Launder and Tselepidakis is considered, together with the model of Merci and Dick for turbulent dissipation. Results are presented for different swirling and recirculating single-phase and two-phase flows, showing the capabilities of the proposed non-constant C_0 GLM formulations compared to the standard GLM.

I. INTRODUCTION

When considering non-premixed combustion the correct description of mixing between fuel and oxidizer is a key issue. The definition of a passive scalar with value 1 in the fuel stream, and 0 in the oxidizer stream (mixture fraction) is useful in order to represent this mixing process. The effect of molecular mixing, enhanced by the stretching of iso-scalar surfaces due to turbulent motion, has been an important research topic in particular for the development of so-called micro-mixing models, starting with the widely used Least Mean Square Estimate (LMSE) model proposed by Dopazo and O'Brien[1].

When simply considering passive scalar mixing in terms of the mean field, the modeling issues are related to the transport and stretching of iso-scalar surfaces by turbulent motion. In this case, the correlations between turbulent velocity fluctuations and scalar values are crucial in order to describe this turbulent transport.

In the same way, when considering dispersed two-phase flows, the dispersion of particles is also a main issue. In the limit of tracer particles, the problem corresponds to the turbulent transport of a non-mixing passive scalar, with no molecular mixing contribution, but where the correlation between velocity fluctuations and tracer particle concentration is a key modeling issue.

In the framework of RANS modeling, both problems can be treated at the level of the one-point joint probability density functions (PDF) of velocity and scalar (mixture fraction in single-phase flows, or particle concentration in dispersed two-phase flows). The joint PDF transport equation can be modeled and solved using a particle stochastic approach[2], where the turbulent flow with passive scalar is represented by a set of stochastic particles. In such Lagrangian methods, each stochastic particle can be seen as a possible realization of the turbulent flow at a given Eulerian point (a given turbulent velocity and passive scalar or tracer concentration). The ensemble of stochastic particles at a given point models the joint velocity-scalar PDF.

It was shown that when a Generalized Langevin Model (GLM) is used for the Lagrangian modeling of stochastic particle velocity evolution, the implied Eulerian modeling of the velocity correlations (Reynolds stresses) corresponds to second-moment closure models[4]. It is a useful way to derive consistent and realizable second-moment closures[5]. It was shown that the Langevin model can be specified such that it corresponds to a given Reynolds-stress model[4,6]

More recently, additional constraints were applied to the GLM coefficients such that a chosen turbulent scalar-flux model was implied (still in correspondence with a chosen Reynolds-stress model)[7]. In particular, it was shown that the usual micro-mixing models, like the widely used LMSE model, generally imply a contribution to the pressure-scrambling term in turbulent scalar-flux modeled transport equations. In order to remove this dependency of the implied turbulent scalar-flux model on the micro-mixing model, a "non-constant C_0 formulation" of the GLM was proposed.

The diffusion coefficient C_0 in the GLM was first identified as a Kolmogorov constant (from considerations on the Lagrangian velocity structure function which should be isotropic and linear in the dissipation rate in the inertial range). Although the most commonly used GLM formulations are constant C_0 formulations, other forms of the GLM have been proposed where C_0 is not a constant, as for instance the IPMb model[4,5], corresponding to the LRR-IP Reynolds-stress model. The choice for a non-constant value for the coefficient C_0 is justified considering that the value of C_0 is actually Reynolds number dependent: it increases with the Reynolds

[a)] Electronic mail: bertrand.naud@ciemat.es

number and approaches an asymptotic value $C_0(\infty)$[8]. The usual value $C_0 = 2.1$ obtained for a moderate Reynolds number flow is probably two to three times lower than the value $C_0(\infty)$ in high Reynolds number flows[9]. Note that the choice of the constant value $C_0 = 2.1$ was determined by Anand and Pope[10] by considering the evolution of the thermal wake behind a line source in grid turbulence (moderate Reynolds number), but more recently, Viswanathan and Pope[11] also obtained good results with the constant value $C_0 = 3$.

It was also shown that the contribution of standard micro-mixing models, together with the constant value $C_0 = 2.1$ in the GLM, implied turbulent scalar-flux models in good correspondence with standard Monin's return-to-isotropy[12] model in the pressure-scrambling term. However, it was observed that without the micro-mixing model contribution, the GLM-implied turbulent scalar-flux model would be quite different[7].

This observation is particularly relevant for dispersed two-phase flow Lagrangian modeling based on a two-phase SLM[13,14]. Such models are indeed built on a constant C_0 GLM formulation (the Simplified Langevin Model, SLM) for the fluid velocity along dispersed particle paths ("seen velocity"). The idea of proposing a two-phase GLM as an extension of the two-phase SLM –one of the recommendations given by Minier *et al.*[15]– was recently considered by Innocenti *e*t al.[16] in the case of the LRR-IP Reynolds-stress model. However, both two-phase SLM and two-phase GLM contain the limitations of their single-phase model counterparts. In the limit of tracer particles, the Lagrangian evolution of the stochastic particles representing the dispered phase directly follows the SLM or GLM. Since there is no molecular mixing contribution in this case, the standard constant $C_0 = 2.1$ leads to a too low constant value for Monin's return-to-isotropy term in the implied turbulent scalar-flux model for tracer particles[17]. Therefore, the development of a two-phase GLM based on the proposed non-constant C_0 GLM formulation would be useful to imply the correct mean dispersion of tracer particles.

The aim of this paper is to extend the non-constant C_0 GLM formulation already proposed by Naud *et al.*[7] to a two-phase GLM for the seen velocity, in order to improve the modeling capabilities of this class of two-phase flow dispersion models in the limit of tracer particles. We first recall the non-constant C_0 GLM general formulation and, in the purpose of having a self-contained presentation, we repeat the theoretical framework detailed in particular by Pope[2,4] for single-phase flows and by Minier and Peirano[13] for dispersed two-phase flows. Following the footsteps of Haworth and Pope[3], we actually use the extension of Wouters *et al.*[6] in order to allow a GLM representation for the Cubic Quasi-Isotropic Reynolds-stress model of Fu, Launder and Tselepidakis[18] (FLT model). We then propose a new two-phase GLM based on this non-constant C_0 GLM for the modeling of the fluid velocity seen by dispersed particles. Finally, different turbulent jets are considered in order to show the capabilities of the proposed models and to illustrate how they overcome the limitations of the constant C_0 formulations for scalar mixing and particle dispersion. First, a single-phase swirling jet and a single-phase jet with recirculation are modeled in order to consider passive scalar mixing. Finally, a polydispersed particle laden jet with recirculation is considered in order to focus on particle dispersion.

II. ONE-POINT JOINT VELOCITY-SCALAR PDF

A. Statistical description at one point

The turbulent flow is described statistically in terms of the joint one-point probability density function (PDF) $f_{\boldsymbol{\Phi}}$ of property vector $\boldsymbol{\Phi}$, such that $f_{\boldsymbol{\Phi}}(\boldsymbol{\Psi};\boldsymbol{x},t)\,.\mathrm{d}\boldsymbol{\Psi}$ is the probability that $\boldsymbol{\Phi}$ is in the interval $[\boldsymbol{\Psi},\boldsymbol{\Psi}+\mathrm{d}\boldsymbol{\Psi}[$ at point $(\boldsymbol{x},t)$. The joint PDF is defined as[2,19]: $f_{\boldsymbol{\Phi}}(\boldsymbol{\Psi};\boldsymbol{x},t) = \langle\delta[\boldsymbol{\Phi}(\boldsymbol{x},t)-\boldsymbol{\Psi}]\rangle$, where $\delta[\,]$ is the Dirac delta function and where the brackets $\langle\,\rangle$ refer to the expected value[19]. Using the conditional expected value[2], $\langle Q(\boldsymbol{x},t)|\boldsymbol{\Psi}\rangle f_{\boldsymbol{\Phi}}(\boldsymbol{\Psi};\boldsymbol{x},t) = \langle Q(\boldsymbol{x},t)\,.\delta[\boldsymbol{\Phi}(\boldsymbol{x},t)-\boldsymbol{\Psi}]\rangle$, mean values (or expected values) $\overline{Q}$ and fluctuations q' are defined as:

$$\overline{Q} = \langle Q(\boldsymbol{x},t)\rangle = \int_{[\boldsymbol{\Psi}]}\langle Q(\boldsymbol{x},t)|\boldsymbol{\Psi}\rangle f_{\boldsymbol{\Phi}}(\boldsymbol{\Psi};\boldsymbol{x},t)\,.\mathrm{d}\boldsymbol{\Psi}$$
$$q' = Q-\overline{Q}. \tag{1}$$

For variable density flows, it is useful to consider the joint mass density function (MDF) $\mathscr{F}_{\boldsymbol{\Phi}}(\boldsymbol{\Psi}) = \rho(\boldsymbol{\Psi})\,f_{\boldsymbol{\Phi}}(\boldsymbol{\Psi})$. Density weighted averages (Favre averages) can be considered:

$$\widetilde{Q} = \frac{\langle\rho(\boldsymbol{x},t)\,Q(\boldsymbol{x},t)\rangle}{\langle\rho(\boldsymbol{x},t)\rangle} = \frac{\int_{[\boldsymbol{\Psi}]}\langle Q(\boldsymbol{x},t)|\boldsymbol{\Psi}\rangle\mathscr{F}_{\boldsymbol{\Phi}}(\boldsymbol{\Psi};\boldsymbol{x},t)\,.\mathrm{d}\boldsymbol{\Psi}}{\int_{[\boldsymbol{\Psi}]}\mathscr{F}_{\boldsymbol{\Phi}}(\boldsymbol{\Psi};\boldsymbol{x},t)\,.\mathrm{d}\boldsymbol{\Psi}}. \tag{2}$$

Fluctuations with respect to the Favre average are defined as: $q'' = Q-\widetilde{Q}$.

B. Joint velocity-scalar PDF

We consider a conserved scalar Z in order to describe mixing. The statistical description of mixing can be made in terms of the joint velocity-composition MDF $\mathscr{F}_{UZ}$. Neglecting the mean viscous stress tensor gradient $\partial\langle\tau_{ij}\rangle/\partial x_j$, the exact transport equation for the joint velocity-composition MDF reads:

$$\begin{aligned}\frac{\partial\mathscr{F}_{UZ}}{\partial t} + V_j\frac{\partial\mathscr{F}_{UZ}}{\partial x_j} + \left(-\frac{1}{\langle\rho\rangle}\frac{\partial\langle p\rangle}{\partial x_i}+g_i\right)\frac{\partial\mathscr{F}_{UZ}}{\partial V_i} \\ = -\frac{\partial}{\partial V_i}\left[\langle a_i|\boldsymbol{V},\zeta\rangle\mathscr{F}_{UZ}\right] \\ -\frac{\partial}{\partial\zeta}\left[\underbrace{\frac{1}{\rho(\zeta)}\left\langle -\frac{\partial J_j^Z}{\partial x_j}\middle|\boldsymbol{V},\zeta\right\rangle}_{\langle\theta_Z|\boldsymbol{V},\zeta\rangle,\text{ with }\theta_Z\text{ the mixing model}}\mathscr{F}_{UZ}\right].\end{aligned} \tag{3}$$

The Lagrangian model for velocity evolution a_i and the mixing model θ_Z close the transport equation for the joint velocity-composition MDF, and therefore imply models for its first statistical moments: the Reynolds stresses $\widetilde{u_i''u_j''}$ and the turbulent scalar fluxes $\widetilde{u_i''Z''}$. In Section II E the LMSE micro-mixing model of Dopazo and O'Brien[1] will be given as example but the theory developed here is for general micro-mixing models θ_Z.

No reaction term appears in the above equation since Z is a conserved scalar. The terms on the left hand side of Eq. (3) appear in closed form: effects of convection and mean pressure gradient are exactly accounted for. The first unclosed term on the right hand side reads:

$$\langle a_i | \boldsymbol{V}, \zeta \rangle = \left(\frac{1}{\langle \rho \rangle} - \frac{1}{\rho(\zeta)} \right) \frac{\partial \langle p \rangle}{\partial x_i} + \frac{1}{\rho(\zeta)} \left\langle -\frac{\partial p'}{\partial x_i} + \frac{\partial \tau'_{ij}}{\partial x_j} \middle| \boldsymbol{V}, \zeta \right\rangle. \quad (4)$$

The modeling of this term is considered here using a Generalized Langevin Model (GLM) a_i[3]:

$$a_i dt = G_{ij} u_j dt + \sqrt{C_0 \varepsilon} dW_i, \quad (5)$$

where dW_i is an increment over dt of the Wiener process W_i. The matrix $G_{ij} = G_{ij}^{(s)} + G_{ij}^{(r)}$ is the sum of two contributions related to the modeling of the slow and rapid terms in the pressure-strain correlation, respectively:

$$G_{ij}^{(s)} = \frac{\varepsilon}{k} \left(\alpha_1 \delta_{ij} + \alpha_2 b_{ij} + \alpha_3 b_{ij}^2 \right), \quad (6)$$

$$G_{ij}^{(r)} = H_{ijkl} \frac{\partial \widetilde{U}_k}{\partial x_l}, \quad (7)$$

$$\begin{aligned} \text{with} \quad H_{ijkl} = {} & \beta_1 \delta_{ij} \delta_{kl} + \beta_2 \delta_{ik} \delta_{jl} + \beta_3 \delta_{il} \delta_{jk} \\ & + \gamma_1 \delta_{ij} b_{kl} + \gamma_2 \delta_{ik} b_{jl} + \gamma_3 \delta_{il} b_{jk} \\ & + \gamma_4 b_{ij} \delta_{kl} + \gamma_5 b_{ik} \delta_{jl} + \gamma_6 b_{il} \delta_{jk} \\ & + \xi_1 b_{ij} b_{kl} + \xi_2 b_{ik} b_{jl} + \xi_3 b_{il} b_{jk}, \end{aligned} \quad (8)$$

with the anisotropy tensor b_{ij} defined in Table I, such that the choice of the coefficients α_i, β_i, γ_i and ξ_i together with the choice of the coefficient C_0 define the specific form of the GLM. Note that the ξ_i terms in (8) were added by Wouters *et al.*[6] to the original formalism of Haworth and Pope[3], in order to allow GLM representations of Reynolds-stress models that include terms which are cubic in b_{ij}.

TABLE I. Useful tensors and scalar invariants

$b_{ij} = \frac{\widetilde{u_i u_j}}{\widetilde{u_l u_l}} - \frac{1}{3}\delta_{ij}$	$S_{ij} = \frac{1}{2}\frac{k}{\varepsilon}\left(\frac{\partial \widetilde{U}_i}{\partial x_j} + \frac{\partial \widetilde{U}_j}{\partial x_i}\right)$	$I_0 = S_{ll}$
$b_{ij}^2 = b_{il} b_{lj}$	$W_{ij} = \frac{1}{2}\frac{k}{\varepsilon}\left(\frac{\partial \widetilde{U}_i}{\partial x_j} - \frac{\partial \widetilde{U}_j}{\partial x_i}\right)$	$I_1 = S_{lm} b_{ml}$
$b_{ij}^3 = b_{ik} b_{km} b_{mj}$	$\frac{P_k}{\varepsilon} = -2\left(I_1 + \frac{1}{3} I_0\right)$	$I_2 = S_{lm} b_{ml}^2$
$F = \left[1 - \frac{9}{2} b_{ll}^2 + 9 b_{ll}^3\right]$		$I_3 = S_{lm} b_{ml}^3$

The matrix G_{ij} can also be written in terms of the tensors and scalar invariants given in Table I, where $k = \frac{1}{2}\widetilde{u''_k u''_k}$ is the turbulent kinetic energy and ε the modeled turbulent dissipation:

$$\begin{aligned} \frac{k}{\varepsilon} G_{ij} = {} & \alpha_1^* \delta_{ij} + \alpha_2^* b_{ij} + \alpha_3 b_{ij}^2 \\ & + (\beta_2 + \beta_3) S_{ij} + (\beta_2 - \beta_3) W_{ij} \\ & + (\gamma_2 + \gamma_3) S_{il} b_{lj} + (\gamma_2 - \gamma_3) W_{il} b_{lj} \\ & + (\gamma_5 + \gamma_6) b_{il} S_{lj} + (\gamma_5 - \gamma_6) b_{il} W_{lj} \\ & + (\xi_2 + \xi_3) b_{il} S_{lm} b_{mj} + (\xi_2 - \xi_3) b_{il} W_{lm} b_{mj}, \end{aligned} \quad (9)$$

where we introduced:

$$\alpha_1^* = \alpha_1 + \beta_1 I_0 + \gamma_1 I_1 \text{ and } \alpha_2^* = \alpha_2 + \gamma_4 I_0 + \xi_1 I_1. \quad (10)$$

When Eq. (3) is modeled and solved using a particle stochastic approach[2], a set of uniformly distributed computational particles evolves according to stochastic differential equations. Each particle has a set of properties $\{w^\star, m^\star, \boldsymbol{X}^\star, Z^\star, \boldsymbol{u}^\star\}$ where $w^\star$ is a numerical weight, $m^\star$ is the mass of the particle, $\boldsymbol{X}^\star$ its position, $Z^\star$ the particle's conserved scalar and $\boldsymbol{u}^\star$ its fluctuating velocity (where the superscript $\star$ denotes that the quantity is a computational particle property). Particle mass $m^\star$ is constant in time.

Solving the following Lagrangian equations for the ensemble of particles:

$$dX_i^\star = U_i^\star dt \qquad \text{with} \qquad U_i^\star = \left[\widetilde{U}_i\right]^\star + u_i^\star, \quad (11)$$

$$dZ^\star = \theta_Z^\star dt, \quad (12)$$

$$du_i^\star = -u_j^\star \left[\frac{\partial \widetilde{U}_i}{\partial x_j}\right]^\star dt + \left[\frac{1}{\overline{\rho}} \frac{\partial \overline{\rho} \widetilde{u''_i u''_j}}{\partial x_j}\right]^\star dt + a_i^\star dt, \quad (13)$$

is equivalent to solving Eq. (3) for the particle joint velocity-scalar MDF $\mathscr{F}_{UZ}^P$:

$$\begin{aligned} & \mathscr{F}_{UZ}^P(\boldsymbol{x}, \boldsymbol{V}, \zeta; t) \\ & = \left\langle \sum_\star w^\star m^\star . \delta(\boldsymbol{X}^\star(t) - \boldsymbol{x}) . \delta(\boldsymbol{U}^\star(t) - \boldsymbol{V}) . \delta(Z^\star(t) - \zeta) \right\rangle. \end{aligned} \quad (14)$$

In the above equations, the quantities between brackets $[\ ]^\star$ are interpolated at the particle location, and the mean density $\overline{\rho}$ and mean velocity vector $\widetilde{\boldsymbol{U}}$ satisfy the mean continuity and mean momentum Reynolds-averaged Navier-Sotkes (RANS) equations:

$$\frac{\partial \overline{\rho}}{\partial t} + \frac{\partial \overline{\rho} \widetilde{U}_j}{\partial x_j} = 0, \quad (15)$$

$$\frac{\partial \overline{\rho} \widetilde{U}_i}{\partial t} + \frac{\partial \overline{\rho} \widetilde{U}_i \widetilde{U}_j}{\partial x_j} = -\frac{\partial \overline{p}}{\partial x_i} - \frac{\partial \overline{\rho} \widetilde{u''_i u''_j}}{\partial x_j} + \overline{\rho} g_i. \quad (16)$$

Hybrid methods[20–22] where the mean velocity and mean pressure gradient are directly obtained from (15) and (16) (for instance using a Finite-Volume method) present the advantage of greatly reducing numerical errors related to the particle method[20], in particular the bias error. This is the method used in the computer code PDFD, originally developed at TU Delft, where moreover the Reynolds stresses $\widetilde{u''_i u''_j}$ are modeled and solved using a second-moment closure consistent with the GLM a_i, while an extra modeled transport equation for the turbulent dissipation ε is provided[22].

C. Reynolds stresses

The Reynolds-stress transport equation reads:

$$\frac{\partial \overline{\rho}\widetilde{u_i''u_j''}}{\partial t}+\frac{\partial \overline{\rho}\widetilde{u_i''u_j''}\widetilde{U}_k}{\partial x_k}=-\overline{\rho}\left(\widetilde{u_i''u_k''}\frac{\partial \widetilde{U}_j}{\partial x_k}+\widetilde{u_j''u_k''}\frac{\partial \widetilde{U}_i}{\partial x_k}\right)+\mathscr{T}_{ij}+\overline{\rho}\Pi_{ij}-\frac{2}{3}\varepsilon\delta_{ij}, \tag{17}$$

where the pressure-strain correlation model Π_{ij} implied by the GLM reads:

$$\Pi_{ij}=\left(\frac{2}{3}+C_0\right)\varepsilon\delta_{ij}+G_{il}\widetilde{u_l u_j}+G_{jl}\widetilde{u_l u_i}. \tag{18}$$

When directly solving Eq. (17) together with Eq. (15) and (16) by means of a Finite-Volume method, we will model the triple correlation term $-\partial\overline{\rho u_i''u_j''u_k''}\big/\partial x_k$ using the Daly-Harlow generalized gradient diffusion model:

$$\mathscr{T}_{ij}=-\frac{\partial}{\partial x_k}\left[C_s\overline{\rho}\frac{k}{\varepsilon}\widetilde{u_k''u_l''}\frac{\partial \widetilde{u_i''u_j''}}{\partial x_l}\right]\quad \text{with } C_s=0.22. \tag{19}$$

This implies a small inconsistency compared to solving Eq. (3) with the GLM as model for velocity evolution, Eq. (5), since in this case the model for the triple correlation term $\mathscr{T}_{ij}$ would directly result from the GLM. However, the differences are small[22] since the pressure-strain correlation modeling is consistent, while low bias errors are induced in the particle method.

D. Mean scalar and scalar variance

Equation (3) implies the following modeled transport equations for the mean scalar $\widetilde{Z}$ and its variance $\widetilde{Z''^2}$:

$$\frac{\partial \overline{\rho}\widetilde{Z}}{\partial t}+\frac{\partial \overline{\rho}\widetilde{U}_j\widetilde{Z}}{\partial x_j}=-\frac{\partial \overline{\rho}\widetilde{u_j''Z''}}{\partial x_j}+\underbrace{\overline{\rho\theta_Z}}_{=0}, \tag{20}$$

$$\frac{\partial \overline{\rho}\widetilde{Z''^2}}{\partial t}+\frac{\partial \overline{\rho}\widetilde{U}_j\widetilde{Z''^2}}{\partial x_j}+2\overline{\rho}\widetilde{u_j''Z''}\frac{\partial \widetilde{Z}}{\partial x_j}=-\frac{\partial \overline{\rho}\widetilde{u_j''Z''^2}}{\partial x_j}-\underbrace{2\overline{\rho Z''\theta_Z}}_{\text{scalar dissipation rate } \overline{\rho}\widetilde{\chi}}. \tag{21}$$

Basic requirements for mixing models θ_Z (second unclosed term in equation (3)) is that they should conserve the mean of the scalar and that they should imply the correct scalar variance decay: these properties are reflected in the last terms of the above transport equations. Most mixing models imply a scalar dissipation rate $\widetilde{\chi}$ modeled as: $\widetilde{\chi}=C_\phi\omega\widetilde{Z''^2}$ (with $\omega=\varepsilon/k$). In this paper, we use the value $C_\phi=2$.

In agreement with a high Reynolds number assumption, no molecular diffusion contributions appear in the above equations, since they are not considered in the mixing model θ_Z. This condition is in line with Taylor's idea that the dispersion of a conserved passive scalar is determined by the motion of fluid particles following the continuous fluid without diffusion. However, we will now see that the turbulent scalar fluxes $\widetilde{u_j''Z''}$ and the triple correlations $\widetilde{u_j''Z''^2}$ in Equations (20) and (21) do generally depend on the choice of the mixing model. Therefore, the evolution of the mean $\widetilde{Z}$ and variance $\widetilde{Z''^2}$ will depend on the choice of the mixing model.

E. Turbulent scalar fluxes

The exact turbulent scalar-flux transport equation for high Reynolds number flows reads:

$$\frac{\partial \overline{\rho}\widetilde{u_i''Z''}}{\partial t}+\frac{\partial \overline{\rho}\widetilde{u_i''Z''}\widetilde{U}_j}{\partial x_j}+\overline{\rho}\widetilde{u_j''Z''}\frac{\partial \widetilde{U}_i}{\partial x_j}+\overline{\rho}\widetilde{u_i''u_j''}\frac{\partial \widetilde{Z}}{\partial x_j}=-\overline{Z\frac{\partial p}{\partial x_i}}-\frac{\partial \overline{\rho u_i''u_j''Z''}}{\partial x_j}. \tag{22}$$

Eq. (3) implies the above equation with the following model for the pressure-scrambling term:

$$-\overline{Z\frac{\partial p}{\partial x_i}}=\overline{\rho}\widetilde{u_i''\theta_Z}+\overline{\rho}\widetilde{a_i Z''}. \tag{23}$$

We introduce a factor C_ϕ^*, in order to write the first term as:

$$\overline{\rho}\widetilde{u_i''\theta_Z}=C_\phi^*\left[\overline{\rho}\frac{\varepsilon}{k}\widetilde{u_i''Z''}\right]. \tag{24}$$

It is important to note that for some mixing models which are conditional on velocity this term is zero[23,24] ($C_\phi^*=0$), as required by Taylor at high Reynolds number. However, this is not the case for most of the standard mixing models, derived in the context of scalar PDF modeling (and not joint velocity-scalar PDF). For instance, the widely used LMSE model[1,25], defined as $\theta_Z^\star=-\frac{1}{2}C_\phi\omega(Z^\star-[\widetilde{Z}]^\star)$, implies a constant value $C_\phi^*=-\frac{1}{2}C_\phi$.

The GLM-implied model for the pressure-scrambling term can be written as[4]:

$$-\overline{Z\frac{\partial p}{\partial x_i}}=-\overline{\rho}\left(-C_\phi^*-\alpha_1\right)\frac{\varepsilon}{k}\widetilde{u_i''Z''}+\overline{\rho}\left(G_{ij}-\alpha_1\frac{\varepsilon}{k}\delta_{ij}\right)\widetilde{u_j''Z''}. \tag{25}$$

This differential turbulent scalar-flux model can be compared to the widely used "standard model":

$$-\overline{Z\frac{\partial p}{\partial x_i}}=-\overline{\rho}C_{\phi 1}\frac{\varepsilon}{k}\widetilde{u_i''Z''}+\overline{\rho}C_{\phi 2}\widetilde{u_j''Z''}\frac{\partial \widetilde{U}_i}{\partial x_j}, \tag{26}$$

where the first term is modeled using Monin's return-to-isotropy[12] with $C_{\phi 1}=3$, and the second term is the destruction of production model by Launder[26] with $C_{\phi 2}=0.5$.

In a similar way as for the Reynolds stresses, when directly solving (22) by means of a Finite-Volume method, the triple correlation term $-\partial\overline{\rho u_i'' u_j'' Z''}\Big/\partial x_j$ will be modeled as:

$$\mathscr{T}_i^Z = -\frac{\partial}{\partial x_j}\left[C_s^Z \overline{\rho}\frac{k}{\varepsilon}\widetilde{u_j'' u_k''}\frac{\partial \widetilde{u_i'' Z''}}{\partial x_k}\right], \quad \text{with } C_s^Z = 0.22. \quad (27)$$

III. GLM-IMPLIED REYNOLDS STRESSES AND TURBULENT SCALAR FLUXES

A. Implied Reynolds-stress model

We consider Reynolds-stress models where the modeled pressure-strain correlation can be expressed in terms of ten tensors $T_{ij}^{(n)}$ as:

$$\Pi_{ij} = \varepsilon \sum_{n=1}^{10} A^{(n)} T_{ij}^{(n)}, \quad (28)$$

where the nondimensional, symmetric, deviatoric tensors $T_{ij}^{(n)}$ are given in Table II.

TABLE II. Nondimensional, symmetric, deviatoric tensors $T_{ij}^{(n)}$

$T_{ij}^{(1)}$	$= b_{ij}$	$T_{ij}^{(6)}$	$= S_{il}b_{lj}^2 + S_{jl}b_{li}^2 - \frac{2}{3}I_2\delta_{ij}$
$T_{ij}^{(2)}$	$= b_{ij}^2 - \frac{1}{3}b_{ll}^2\delta_{ij}$	$T_{ij}^{(7)}$	$= W_{il}b_{lj}^2 + W_{jl}b_{li}^2$
$T_{ij}^{(3)}$	$= S_{ij} - \frac{1}{3}I_0\delta_{ij}$	$T_{ij}^{(8)}$	$= b_{il}S_{lm}b_{mj} - \frac{1}{3}I_2\delta_{ij}$
$T_{ij}^{(4)}$	$= S_{il}b_{lj} + S_{jl}b_{li}$ $-\frac{2}{3}I_1\delta_{ij}$	$T_{ij}^{(9)}$	$= b_{il}^2 W_{lm}b_{mj} + b_{jl}^2 W_{lm}b_{mi}$
		$T_{ij}^{(10)}$	$= b_{il}^2 S_{lm}b_{mj} + b_{jl}^2 S_{lm}b_{mi}$ $-\frac{2}{3}I_3\delta_{ij}$
$T_{ij}^{(5)}$	$= W_{il}b_{lj} + W_{jl}b_{li}$		

Note that we follow the general formalism introduced by Wouters *et al.*[6], extending the formalism of Haworth and Pope[3], such that the trace of the tensors $T_{ij}^{(n)}$ is zero in variable density flows, and where the tensors $T_{ij}^{(9)}$ and $T_{ij}^{(10)}$ (and the GLM coefficients ξ_i) are introduced in order to allow GLM representations of Reynolds-stress models that include terms which are cubic in b_{ij}.

The choice of the coefficients α_i, β_i, γ_i and ξ_i of the GLM, implies the coefficients $A^{(n)}$ of the pressure-strain correlation summarized in Table III.

B. GLM in correspondence with a given Reynolds-stress model

As explained by Pope (1994)[4], we now recall how to choose the GLM coefficients in correspondence with a given Reynolds-stress model defined by equation (28). Arbitrary values can be chosen for the parameters β_1, γ_1, γ_4 and ξ_1. This is clear from Eq. (10) which shows that their contributions can be incorporated in the coefficients α_1 and α_2.

TABLE III. Relationship between the coefficients $A^{(n)}$ and the GLM parameters

$A^{(1)}$	$= 4\alpha_1^* + \frac{4}{3}\alpha_2^* + 2b_{kk}^2\alpha_3$
$A^{(2)}$	$= 4\alpha_2^* + \frac{4}{3}\alpha_3$
$A^{(3)}$	$= \frac{4}{3}(\beta_2 + \beta_3)$
$A^{(4)}$	$= 2(\beta_2 + \beta_3) + \frac{2}{3}(\gamma_2 + \gamma_3 + \gamma_5 + \gamma_6)$
$A^{(5)}$	$= 2(\beta_2 - \beta_3) + \frac{2}{3}(\gamma_2 - \gamma_3 - \gamma_5 + \gamma_6)$
$A^{(6)}$	$= 2(\gamma_2 + \gamma_3)$
$A^{(7)}$	$= 2(\gamma_2 - \gamma_3)$
$A^{(8)}$	$= 4(\gamma_5 + \gamma_6) + \frac{4}{3}(\xi_3 + \xi_2)$
$A^{(9)}$	$= 2(\xi_3 - \xi_2)$
$A^{(10)}$	$= 2(\xi_3 + \xi_2)$

Note that the GLM satisfies the condition (see Table III):

$$\frac{3}{2}A^{(3)} - A^{(4)} + \frac{1}{3}A^{(6)} + \frac{1}{6}A^{(8)} - \frac{1}{9}A^{(10)} = 0. \quad (29)$$

A given Reynolds-stress model needs to satisfy this relation in order to have a GLM representation. Eq. (29) implies that the expressions for $A^{(3)}$–$A^{(10)}$ in Table III only provide seven independent relations for eight parameters: β_2, β_3, γ_2, γ_3, γ_5, γ_6, ξ_2 and ξ_3. Introducing the parameter β^*:

$$\beta^* = \frac{1}{4}A^{(5)} - \frac{1}{12}A^{(7)} - \frac{1}{24}A^{(8)} + \frac{1}{36}A^{(10)} + \frac{1}{3}\gamma_5, \quad (30)$$

we can express the parameters β_2, β_3, γ_2, γ_3, γ_5, γ_6, ξ_2, ξ_3 of the GLM as function of the coefficients $A^{(3)}$–$A^{(10)}$ (see Table IV). The value $\beta^* = \frac{1}{2}$ was proposed since it leads to $\beta_2 - \beta_3 = 1$ as required in isotropic turbulence[3,4].

In order to determine the four remaining GLM coefficients α_1, α_2, α_3 and C_0, we use the two relations for $A^{(1)}$ and $A^{(2)}$ from Table III, together with the third condition that the redistribution term in the pressure-strain correlation does not affect the turbulent kinetic energy, where the latter condition can be written as[4,7]:

$$-\left(\frac{1}{2} + \frac{3}{4}C_0\right) + \frac{F}{3}\alpha_2^* = A^*, \quad (31)$$

where

$$A^* = \frac{1}{4}\left[A^{(1)} + A^{(2)}\left(-\frac{1}{2}b_{kk}^2 + 3b_{kk}^3\right) + A^{**}\right], \quad (32)$$
$$A^{**} = A^{(3)}I_0 + 2A^{(4)}I_1 + \left(2A^{(6)} + A^{(8)}\right)I_2 + 2A^{(10)}I_3.$$

A fourth relation is needed. The most common choice is to set a constant value for C_0, usually $C_0 = 2.1$, as detailed in the next paragraph. However, we will see that this choice does not allow to specify the constant of Monin's return-to-isotropy term in the implied turbulent scalar-flux transport equation. This was already pointed out by Durbin and Shabany[17] who proposed an alternative formulation. However, in addition to this issue, the possible contribution of the mixing model when $C_\phi^* \neq 0$ should also be taken into account. The non-constant C_0 formulation of Naud *et al.*[7] which is recalled next allows a GLM representation of a given Reynolds-stress model while specifying the value of the constant in Monin's return-to-isotropy term.

The specification of the GLM coefficients corresponding to a given Reynolds-stress second moment closure defined by equation (28) is summarized in Table IV, both for the constant and the proposed non-constant C_0 formulations.

TABLE IV. Summary of the coefficients of the GLM in correspondence with a given Reynolds-stress model defined by equation (28), both for the constant and the proposed variable C_0 formulations.

β_*	$=$ = 0.5		
β_1	$=$ arbitrary = β_2	γ_1	$=$ arbitrary = γ_5
ξ_1	$=$ arbitrary = ξ_2	γ_4	$=$ arbitrary = γ_2
β_2	$= \frac{3}{8}A^{(3)}+\beta^*$	γ_2	$= \frac{1}{4}\left(A^{(6)}+A^{(7)}\right)$
β_3	$= \frac{3}{8}A^{(3)}-\beta^*$	γ_3	$= \frac{1}{4}\left(A^{(6)}-A^{(7)}\right)$
ξ_2	$= \frac{1}{4}\left(A^{(10)}-A^{(9)}\right)$	γ_5	$=$ from Eq. (30)
ξ_3	$= \frac{1}{4}\left(A^{(10)}+A^{(9)}\right)$	γ_6	$= \frac{1}{4}A^{(8)}-\frac{1}{6}A^{(10)}-\gamma_5$
	Constant C_0		Non-constant C_0
α_2^*	$=$ from Eq. (33)		from Eq. (36)
α_3	$=$ from Eq. (34)		from Eq. (37)
α_1^*	$=$ from Eq. (35)		from Eq. (38)
C_0	$=$ 2.1		from Eq. (39)

C. GLM-implied turbulent scalar fluxes

Standard GLM formulation with constant C_0 The most commonly used GLM formulations[4] use a constant value for C_0 as fourth condition, with $C_0 = 2.1$[10]. From the expressions for $A^{(1)}$ and $A^{(2)}$ given in Table III and Eq. (31), we can obtain the parameters α_1^*, α_2^* and α_3:

$$\alpha_2^* = \frac{3}{F}\left[\left(\frac{1}{2}+\frac{3}{4}C_0\right)+A^*\right], \tag{33}$$

$$\alpha_3 = \frac{3}{4}A^{(2)} - 3\alpha_2^*, \tag{34}$$

$$\alpha_1^* = \frac{1}{4}A^{(1)} - \frac{1}{3}\alpha_2^* - \frac{1}{2}b_{kk}^2\alpha_3. \tag{35}$$

However, this formulation implies a turbulent scalar-flux model where the pressure-scrambling term, given by Eq. (25) is dependent on C_ϕ^*, and may imply a value $(-C_\phi^* - \alpha_1)$ quite different from the Monin's constant value for the return-to-isotropy contribution.

For instance, in the case of isotropic turbulence for a constant density flow, $-\alpha_1 = \left(\frac{1}{2}+\frac{3}{4}C_0\right) = 2.075$. When $C_\phi^* = 0$, this constant value of 2.075 in the return-to-isotropy term in (25) will therefore be quite different from the standard value $C_{\phi 1} = 3$. On the other hand, as noticed by Naud *et al.*[7], it is quite remarkable that the contribution of a standard mixing model as LMSE (where $C_\phi^* = 1$ when using the standard value $C_\phi = 2$ for scalar dissipation rate modeling) will lead to a value of 3.075. This suggests that so far, in transported joint velocity-composition PDF calculations, the too low value $C_0 = 2.1$ together with the typical non-zero values for C_ϕ^*, have implied turbulent scalar-flux models where the modeling of the retrun-to-isotropy term resulted to be in reasonable correspondence with Monin's standard constant value.

Proposed GLM formulation with variable C_0 In the variable C_0 GLM formulation of Naud *et al.*[7], the condition $\alpha_1^* = -C_{\phi 1} - C_\phi^* - \alpha_3 b_{kk}^3$ is required, leading to:

$$\alpha_2^* = \frac{3}{F}\left[C_{\phi 1} + C_\phi^* + \frac{A^{(1)}}{4} + \frac{3}{4}\left(\frac{-1}{2}b_{kk}^2 + b_{kk}^3\right)A^{(2)}\right] \tag{36}$$

$$\alpha_3 = \frac{3}{4}A^{(2)} - 3\alpha_2^*, \tag{37}$$

$$\alpha_1^* = -C_{\phi 1} - C_\phi^* - \alpha_3 b_{kk}^3, \tag{38}$$

$$C_0 = \frac{4}{3}\left[\left(C_{\phi 1}+C_\phi^*\right) - \frac{1}{2} - \frac{1}{4}\left(A^{(2)}b_{kk}^2 + A^{**}\right)\right]. \tag{39}$$

The GLM coefficients given by Eq. (36)-(39) imply a turbulent scalar-flux model with a return-to-isotropy term in correspondence with Monin's model:

$$\begin{aligned} -\overline{Z\frac{\partial p}{\partial x_i}} = &-\overline{\rho} C_{\phi 1}\frac{\varepsilon}{k}\widetilde{u_i''Z''} \\ &-\overline{\rho}\left[\alpha_3 b_{kk}^3\delta_{ij} - \left(\alpha_2^* b_{ij} + \alpha_3 b_{ij}^2\right)\right]\frac{\varepsilon}{k}\widetilde{u_j''Z''} \\ &+\overline{\rho}\left[\beta_2\frac{\partial \widetilde{U}_i}{\partial x_j} + \beta_3\frac{\partial \widetilde{U}_j}{\partial x_i} + \frac{\varepsilon}{k}\Lambda_{ij}\right]\widetilde{u_j''Z''}. \end{aligned} \tag{40}$$

The α_2^* and α_3 terms correspond to non-linear relaxation of the turbulent scalar flux (i.e. anisotropy effects in the scalar-flux decay rate), and Λ_{ij} includes other higher-order contributions:

$$\begin{aligned} \Lambda_{ij} = &(\gamma_2+\gamma_3)S_{il}b_{lj} + (\gamma_5+\gamma_6)S_{jl}b_{li} \\ &+ (\gamma_2-\gamma_3)W_{il}b_{lj} - (\gamma_5-\gamma_6)W_{jl}b_{li} \\ &+ (\xi_2+\xi_3)b_{il}S_{lm}b_{mj} + (\xi_2-\xi_3)b_{il}W_{lm}b_{mj}. \end{aligned} \tag{41}$$

In this case, it is the modeling of Monin's term which determines the value of the coefficient C_0, while the mixing model only affects the α_2^* and α_3 non-linear relaxation terms.

The formulation presented here is slightly different from the one presented by Naud *et al.* since they proposed to use a value $\beta^* = C_{\phi 2} - \frac{3}{8}A^{(3)}$ such that the destruction of production term from equation (26) would appear in (40). However, the value $\beta^* = 0.5$ required in isotropic turbulence implies the β_2 and β_3 terms in Eq. (40) as proposed by Lumley[4,27]. Here, we prefer to keep the value $\beta^* = 0.5$ and let the scalar-flux model being implied by the GLM, while only imposing the return-to-isotropy Monin's term.

In order to ensure $C_0 > 0$ in (39), we follow a similar idea as used by Durbin and Speziale[5] for the IPMb model. Although such situations are highly unlikely[7] (and do not occur in the cases presented at the end of this paper), we add a possible modification of $C_{\phi 1}$, by specifying $C_{\phi 1} = \max[3.0; C_{\phi 1}^0]$, where $C_{\phi 1}^0 = -C_\phi^* + \frac{1}{2} + \frac{1}{4}(A^{(2)}b_{kk}^2 + A^{**})$.

IV. DISPERSED PARTICLE PDF AND PARTICLE DISPERSION MODELING

In order to model particle dispersion in dispersed two-phase flows, Minier and Peirano[13] presented in detail the derivation of a two-phase Langevin model for the velocity of the fluid seen by particles based on the Simplified Langevin model (SLM) with constant C_0. The history of the evolution of such two-phase Langevin models was explained in a detailed description of guidelines for the derivation of both single-phase and two-phase Lagrangian stochastic models[15]. Variants of the model include a modification of the drift term[28], and more recently, stochastic processes in the evolution of the particle velocity[16] are considered in addition to the stochastic model for the seen velocity. We will start here from the formulation of Minier and Peirano[13] without two-way coupling effects, and with the dispersed phase mean properties evaluated as class averages for polydispersed two-phase flows. In the limit of tracer particles, such a two-phase Langevin model is equivalent to the single-phase Langevin formulation. Therefore the modeling of tracer particle dispersion using the two-phase SLM will correspond to the transport of a non-mixing passive scalar, using the turbulent scalar-flux model implied by the constant C_0 SLM formulation.

In the SLM, the matrix G_{ij} is drastically simplified since it includes no rapid contribution ($G_{ij}^{(r)} = 0$), and since the slow term reduces to $\frac{\varepsilon}{k}\alpha_1\delta_{ij}$ (with $\alpha_2 = \alpha_3 = 0$), corresponding to the simple Rotta model for the Reynolds stresses. In this case, we can easily show that the pressure-scrambling term in the implied turbulent scalar-flux model will be:

$$-\overline{Z\frac{\partial p}{\partial x_i}} = -\overline{\rho}\left(\frac{1}{2}+\frac{3}{4}C_0\right)\frac{\varepsilon}{k}\widetilde{u_i''Z''}. \tag{42}$$

The model only includes the return-to-isotropy term where the standard value $C_0 = 2.1$ implies a constant value of 2.075, quite different from the standard Monin's constant value $C_{\phi 1} = 3$. Note that the value $C_0 = 10/3$ should be used in this case in order to imply a return-to-isotropy contribution in correspondence with the standard Monin's term.

In the following, in order to impose the correct Monin's return-to-isotropy model, and in order to possibly consider more sophisticated Reynolds-stress models, the two-phase model of Minier and Peirano[13] is extended based on Naud *et al.*[7] non-constant C_0 GLM.

A. Statistical description of the dispersed phase

Although this description is general for dispersed two-phase flows where the dispersed phase may consist of solid particles or liquid droplets, and where the cases considered may not necessarily be jet-like configurations, we will refer here to the dispersed phase as "spray" and to the dispersed particles as "droplets".

The spray can be described in terms of the discrete joint mass density function of diameter, velocity and seen velocity (droplet MDF):

$$\mathscr{F}_{\mathrm{p}}\left(\boldsymbol{x},\boldsymbol{\Psi}_{\mathrm{p}};t\right) = m_{\mathrm{p}}\left(d_{\mathrm{p}}\right)\left\langle \sum_{+}\delta\left(\boldsymbol{X}_{\mathrm{p}}^{+}-\boldsymbol{x}\right).\delta\left(\boldsymbol{\Phi}_{\mathrm{p}}^{+}-\boldsymbol{\Psi}_{\mathrm{p}}\right)\right\rangle \tag{43}$$

with $\boldsymbol{\Phi}_{\mathrm{p}}^{+} = \left(D_{\mathrm{p}}^{+},\boldsymbol{U}_{\mathrm{p}}^{+},\boldsymbol{U}_{\mathrm{s}}^{+}\right)$, where $\boldsymbol{X}_{\mathrm{p}}^{+}$ is the droplet position vector, D_{p}^{+} the constant droplet diameter, $\boldsymbol{U}_{\mathrm{p}}^{+}$ the droplet velocity and $\boldsymbol{U}_{\mathrm{s}}^{+}$ the fluid velocity seen by the droplet (i.e. the velocity of the undisturbed fluid flow at the position of the droplet center: the velocity that would exist in the absence of the droplet but turbulent and disturbed by all the other droplets[29]). The sample-space vector is $\boldsymbol{\Psi}_{\mathrm{p}} = \left(d_{\mathrm{p}},\boldsymbol{V}_{\mathrm{p}},\boldsymbol{V}_{\mathrm{s}}\right)$.

The sum in Eq. (43) is over the $N_{\mathrm{p}}(t)$ droplets present in the domain at time t, such that $\mathscr{F}_{\mathrm{p}}\left(\boldsymbol{x},\boldsymbol{\Psi}_{\mathrm{p}};t\right).\mathrm{d}\boldsymbol{\Psi}_{\mathrm{p}}$ gives the probable mass of droplets present at $(\boldsymbol{x},t)$ with diameter in the range $[d_{\mathrm{p}}, d_{\mathrm{p}}+\mathrm{d}d_{\mathrm{p}}]$, velocity in $[\boldsymbol{V}_{\mathrm{p}}, \boldsymbol{V}_{\mathrm{p}}+\mathrm{d}\boldsymbol{V}_{\mathrm{p}}]$ and seeing a fluid velocity in $[\boldsymbol{V}_{\mathrm{s}}, \boldsymbol{V}_{\mathrm{s}}+\mathrm{d}\boldsymbol{V}_{\mathrm{s}}]$.

We define a conditional expected values $\langle\ |\ \rangle_{\mathrm{p}}$ as:

$$\begin{aligned}&\left\langle Q_{\mathrm{p}}^{+}\,\middle|\,\boldsymbol{x},\boldsymbol{\Psi}_{\mathrm{p}};t\right\rangle_{\mathrm{p}}\mathscr{F}_{\mathrm{p}}\left(\boldsymbol{x},\boldsymbol{\Psi}_{\mathrm{p}};t\right) \\ &\quad= \left\langle \sum_{+} m_{\mathrm{p}}Q_{\mathrm{p}}^{+}.\delta\left(\boldsymbol{X}_{\mathrm{p}}^{+}-\boldsymbol{x}\right).\delta\left(\boldsymbol{\Phi}_{\mathrm{p}}^{+}-\boldsymbol{\Psi}_{\mathrm{p}}\right)\right\rangle.\end{aligned} \tag{44}$$

In the absence of mass transfer, collisions, coalescence and breakup, the droplet MDF transport equation reads[30]:

$$\begin{aligned}\frac{\partial \mathscr{F}_{\mathrm{p}}}{\partial t} + V_{\mathrm{p},j}\frac{\partial \mathscr{F}_{\mathrm{p}}}{\partial x_j} = &-\frac{\partial}{\partial V_{\mathrm{p},i}}\left[\left\langle \frac{\mathrm{d}U_{\mathrm{p},i}^{+}}{\mathrm{d}t}\,\middle|\,\boldsymbol{x},\boldsymbol{\Psi}_{\mathrm{p}};t\right\rangle_{\mathrm{p}}\mathscr{F}_{\mathrm{p}}\right] \\ &-\frac{\partial}{\partial V_{\mathrm{s},i}}\left[\left\langle \frac{\mathrm{d}U_{\mathrm{s},i}^{+}}{\mathrm{d}t}\,\middle|\,\boldsymbol{x},\boldsymbol{\Psi}_{\mathrm{p}};t\right\rangle_{\mathrm{p}}\mathscr{F}_{\mathrm{p}}\right]\end{aligned} \tag{45}$$

B. Lagrangian modeling of the droplet MDF

In order to model and solve Eq. (45), a particle method is used. A set of uniformly distributed parcels (or computational droplets), each having a position, diameter, velocity and seen velocity, evolves according to stochastic differential equations such that the ensemble provides a numerical approximation of the modeled droplet MDF $\mathscr{F}_{\mathrm{p}}^{P}$.

For the non-evaporating spray considered, each parcel has a set of properties $\{n_{\mathrm{p}}^{\star},\boldsymbol{X}_{\mathrm{p}}^{\star},D_{\mathrm{p}}^{\star},\boldsymbol{U}_{\mathrm{p}}^{\star},\boldsymbol{U}_{\mathrm{s}}^{\star}\}$, where $n_{\mathrm{p}}^{\star}$ is a weight factor associated to the parcel (a parcel is not in one to one correspondence to a "real" droplet: each computational droplet is a statistical sample of the dispersed phase, and the weight factors accommodate the difference between the number of samples and the number of real droplets). The superscript * denotes that the quantity is a stochastic parcel property. The modeled droplet MDF is defined as

$$\mathscr{F}_{\mathrm{p}}^{P}\left(\boldsymbol{x},\boldsymbol{\Psi}_{\mathrm{p}};t\right) = \left\langle \sum_{\star} n_{\mathrm{p}}^{\star}m_{\mathrm{p}}^{\star}.\delta\left(\boldsymbol{X}_{\mathrm{p}}^{\star}(t)-\boldsymbol{x}\right).\delta\left(\boldsymbol{\Phi}_{\mathrm{p}}^{\star}-\boldsymbol{\Psi}_{\mathrm{p}}\right)\right\rangle, \tag{46}$$

where $m_\mathrm{p}^\star = \rho_\mathrm{p}\pi\left(D_\mathrm{p}^\star\right)^3/6$ is the mass of the parcel. Unconditional droplet mean properties in a small domain Ω of volume $\mathscr{V}_\Omega$, are obtained as:

$$\rho_\mathrm{p}\langle Q_\mathrm{p}\rangle = \frac{1}{\mathscr{V}_\Omega}\left\langle \sum_{\star \text{ in } \Omega} n_\mathrm{p}^\star m_\mathrm{p}^\star Q_\mathrm{p}^\star(t)\right\rangle, \tag{47}$$

and conditional averages are obtained as:

$$\langle Q_\mathrm{p}\rangle_\mathrm{p} = \left\langle \sum_{\star \text{ in } \Omega} n_\mathrm{p}^\star m_\mathrm{p}^\star Q_\mathrm{p}^\star(t)\right\rangle \Big/ \left\langle \sum_{\star \text{ in } \Omega} n_\mathrm{p}^\star m_\mathrm{p}^\star \right\rangle. \tag{48}$$

For polydispersed two-phase flows, such conditional averages can be obtained separately for different size classes (class averages)[31]. Note that the droplet volume fraction α can be obtained as an unconditional average as:

$$\alpha = \frac{1}{\rho_\mathrm{p}\mathscr{V}_\Omega}\left\langle \sum_{\star \text{ in } \Omega} n_\mathrm{p}^\star m_\mathrm{p}^\star\right\rangle = \frac{1}{\mathscr{V}_\Omega}\frac{\pi}{6}\left\langle \sum_{\star \text{ in } \Omega} n_\mathrm{p}^\star D_\mathrm{p}^{\star 3}\right\rangle. \tag{49}$$

In order to model and solve equation (45), The stochastic particle position $\boldsymbol{X}_\mathrm{p}^\star$ and velocity $\boldsymbol{U}_\mathrm{p}^\star$ follow the simplified equations of motion[32,33]:

$$\frac{\mathrm{d}X_{\mathrm{p},i}}{\mathrm{d}t} = U_{\mathrm{p},i}, \tag{50}$$

$$m_\mathrm{p}\frac{\mathrm{d}U_{\mathrm{p},i}}{\mathrm{d}t} = m_\mathrm{p}\frac{U_{\mathrm{s},i} - U_{\mathrm{p},i}}{\tau_\mathrm{p}} - \frac{m_\mathrm{p}}{\rho_\mathrm{p}}\frac{\partial\langle p\rangle}{\partial x_i} + m_\mathrm{p} g_i. \tag{51}$$

The effect of the surrounding fluid flow is included through the first two terms on the right hand side of equation (51), respectively the drag force and the mean pressure gradient at the particle location.

The particle response time scale τ_p is given by the response time in a Stokes regime $\tau_\mathrm{p}^{(\mathrm{St})}$:

$$\frac{1}{\tau_\mathrm{p}} = \frac{f_1}{\tau_\mathrm{p}^{(\mathrm{St})}} \qquad \text{with} \qquad \tau_\mathrm{p}^{(\mathrm{St})} = \frac{\rho_\mathrm{p} D_p^2}{18\mu}, \tag{52}$$

where f_1 is the Schiller-Naumann correction for high Reynolds number flows:

$$f_1 = \begin{cases} 1 + 0.15\mathrm{Re}_\mathrm{p}^{0.687} & \text{if } \mathrm{Re}_\mathrm{p} \le 1000 \\ 0.44\dfrac{\mathrm{Re}_\mathrm{p}}{24} & \text{if } \mathrm{Re}_\mathrm{p} > 1000 \end{cases} \tag{53}$$

with

$$\mathrm{Re}_\mathrm{p} = \frac{\rho\left|\boldsymbol{U}_\mathrm{p} - \boldsymbol{U}_\mathrm{s}\right| D_\mathrm{p}}{\mu}, \tag{54}$$

where ρ and μ are the continuous phase density and dynamic molecular viscosity, respectively.

C. Two-phase GLM for dispersed two-phase flows

As a starting point, we consider the two-phase SLM of Minier and Peirano[13], written in terms of the fluctuating seen velocity, defined as the fluctuation with respect to the mean continuous phase velocity interpolated at the parcel location, $u_{\mathrm{s},i}^\star = U_{\mathrm{s},i}^\star - \left[\widetilde{U}_i\right]^\star$:

$$du_{\mathrm{s},i}^\star = -u_{\mathrm{s},j}^\star\left[\frac{\partial\widetilde{U}_i}{\partial x_j}\right]^\star dt + \left[\frac{1}{\overline{\rho}}\frac{\partial\overline{\rho}\widetilde{u_i''u_j''}}{\partial x_j}\right]^\star dt + a_{\mathrm{s},i}^\star dt$$
$$+ \left[\left(\langle U_{\mathrm{r},j}\rangle_\mathrm{p} - U_{\mathrm{r},j}\right)\frac{\partial\widetilde{U}_i}{\partial x_j}\right]^\star dt, \tag{55}$$

such that the conditional average $\langle \boldsymbol{u}_\mathrm{s}\rangle_\mathrm{p}$ is the so-called turbulent drift velocity. The relative velocity $\boldsymbol{U}_\mathrm{r} = \boldsymbol{U}_\mathrm{p} - \boldsymbol{U}_\mathrm{s}$ is the difference between the particle velocity and the seen velocity. For polydispersed flows, equation (55) is written for each size class. This means that the mean relative velocities $\langle \boldsymbol{U}_\mathrm{r}\rangle_\mathrm{p}$ are evaluated for each droplet size class separately (class averages)[31]. We can already see that in the limit of tracer particles, where $\boldsymbol{U}_\mathrm{r} = 0$, the above equation indeed formally relaxes to the single-phase model, (13).

The two-phase SLM of Minier and Peirano[13] can be written as:

$$a_{\mathrm{s},i}dt = \mathscr{H}_{\mathrm{s},il} G_{lj}^{(s)} u_{\mathrm{s},j} dt + B_{\mathrm{s},ij} dW_j, \tag{56}$$

where the matrix $G_{lj}^{(s)}$ corresponds to the Simplified Langevin Model. The first modification to the single-phase SLM is based on the analysis of Csanady[34] in order to account for crossing-trajectory effects due to a mean relative velocity for inertial particles[14], by modifying the timescale in the drift term through the matrix $\mathscr{H}_{\mathrm{s},ij}$:

$$\mathscr{H}_{\mathrm{s},ij} = b_\perp\delta_{ij} + \left[b_\parallel - b_\perp\right] r_i r_j \quad \text{with} \quad r_i = \frac{\langle U_{\mathrm{r},i}\rangle_\mathrm{p}}{\left|\langle \boldsymbol{U}_\mathrm{r}\rangle_\mathrm{p}\right|}, \tag{57}$$

with

$$b_\parallel = \sqrt{1 + c_\beta\xi_\mathrm{r}} \quad \text{and} \quad b_\perp = \sqrt{1 + 4c_\beta\xi_\mathrm{r}}, \tag{58}$$

where $c_\beta = 0.45$ and $\xi_\mathrm{r} = \frac{3}{2}\left|\langle \boldsymbol{U}_\mathrm{r}\rangle_\mathrm{p}\right|^2/k$. The second modification to the single-phase SLM concerns the introduction of the diffusion matrix $B_{\mathrm{s},ij}$ instead of $\sqrt{C_0\varepsilon}\delta_{ij}$, such that:

$$\left(B_\mathrm{s}B_\mathrm{s}^t\right)_{ij} = \varepsilon\left(C_0\lambda\mathscr{H}_{\mathrm{s},ij} + \frac{2}{3}\left(\lambda\mathscr{H}_{\mathrm{s},ij} - \delta_{ij}\right)\right), \tag{59}$$

where the factor λ specified as $\lambda = \frac{3}{2}\mathrm{Tr}(\mathscr{H}_\mathrm{s}\mathscr{R})/[\mathrm{Tr}(\mathscr{H}_\mathrm{s})k]$, where $\mathrm{Tr}(\mathscr{H}_\mathrm{s})$ denotes the trace of matrix $\mathscr{H}_{\mathrm{s},ij}$ and where $\mathscr{R}_{ij} = \widetilde{u_i''u_j''}$ is the Reynolds-stress tensor, such that in homogeneous isotropic decaying turbulence, the turbulent kinetic energy of the fluid along particle paths satisfies: $\frac{1}{2}d\langle u_{\mathrm{s},i}u_{\mathrm{s},i}\rangle_\mathrm{p}/dt = -\varepsilon$. Note that in the two-phase SLM of

Minier and Peirano the diffusion coefficient $B_{\mathrm{s},ij}$ is not a "constant C_0" diffusion coefficient when the mean relative velocity $\langle \boldsymbol{U}_\mathrm{r}\rangle_\mathrm{p}$ is not zero. However, in the limit of tracer particles, we can easily verify that $\mathscr{H}_{\mathrm{s},ij} = \delta_{ij}$ and that the diffusion matrix reduces to $\sqrt{C_0 \varepsilon}\delta_{ij}$.

As an extension of the two-phase SLM of Minier and Peirano, we propose the following two-phase GLM:

$$a_{\mathrm{s},i} dt = \left[\mathscr{H}_{\mathrm{s},il} G^{(s)}_{lj} + G^{(r)}_{ij}\right] u_{\mathrm{s},j} dt + B_{\mathrm{s},ij} dW_j, \qquad (60)$$

where $G^{(s)}_{lj}$, $G^{(r)}_{ij}$ and C_0 follow the general single-phase GLM formulation described in Section III, and where $\mathscr{H}_{\mathrm{s},ij}$ and $B_{\mathrm{s},ij}$ are the same as in the two-phase SLM of Minier and Peirano. Note that this general formulation is similar to the speficic form proposed recently by Innocenti et al.[16], corresponding to the Launder, Reece and Rodi isotropization of production (LRR-IP) Reynolds-stress model. The current formulation is more general in terms of the possible correspondence with a given Reynolds-stress model, but, more importantly for the purpose of this paper, it allows to use the proposed non-constant C_0 formulation in order to correctly model the dispersion of tracer particles.

Two remarks can be made on this model. First, the rapid contribution $G^{(r)}_{ij}$ which is added in (60) for the seen velocity is the same as in the fluid case. This means that for inertial particles, we assume that the modelling of rapid contributions for the seen velocity fluctuations can be the same as in the fluid case. This could of course be discussed, but as explained by Minier et al.[15], the main issue for inertial particles is to retrieve the correct limit of the integral time scale for the velocity of the fluid seen, which is ensured by the modification of the slow term according to Csanady's analysis through $\mathscr{H}_{\mathrm{s},ij}$ defined by (57) and (58).

The second remark is that the diffusion matrix $B_{\mathrm{s},ij}$ is also unchanged, which can be justified since its derivation was obtained such that $\frac{1}{2} d\langle u_{\mathrm{s},i} u_{\mathrm{s},i}\rangle_\mathrm{p}/dt = -\varepsilon$ in homogeneous isotropic decaying turbulence. However, as mentioned by Innocenti et al.[16], in the presence of a mean shear, the anisotropic contributions from $G^{(r)}_{ij}$ could also be considered in the derivation of the diffusion coefficient, which is not included in the present form of the proposed two-phase GLM. As previously mentioned, in the limit of tracer particles, the relative velocity is zero and (60) and (55) reduce respectively to the single-phase equations (5) and (13).

V. APPLICATIONS

In order to illustrate the capabilities of the proposed non-constant C_0 GLM formulations for mean scalar mixing and particle dispersion, we will now consider different complex turbulent jet flows involving either swirl or recirculations. We will first detail the second-moment closure model chosen for the Reynolds stresses.

The computer program PDFD originally developed at TU Delft is used, where the implemented hybrid Finite-Volume / particle method has already been applied to different single-phase and two-phase turbulent non-reacting and reacting flows[35–41]. The second-order accuracy of the method, the use of iteration averages in order to reduce statistical errors in the evaluation of expected values, and the reduction of bias error in this consistent hybrid method are detailed in Naud *et al.*[22].

In all the cases considered, we solve the RANS equations (15), (16), (17) and (61) with the implemented Finite-Volme method. In the single-phase flow cases, for the purpose of this paper, there is no need to solve the joint velocity-scalar PDF transport equation using the particle method. It is enough to solve the mean scalar and variance equations (20) and (21), together with the scalar-flux model implied by the chosen GLM, (22) and (23). In the dispersed two-phase flow case, on the other hand, the droplet MDF transport equation (45) is modeled and solved using the particle method.

A. FLT Reynolds-stress model and turbulent dissipation

In order to correctly deal with swirl and recirculations, the cubic model of Fu, Launder and Tselepidakis (FLT model)[18] is chosen, in combination with Merci and Dick model for turbulent dissipation[42].

TABLE V. Coefficients of the FLT Reynolds-stress model defined by Equation (28), with $Q_1 = I_1 + \frac{1}{3} I_0$ and $Q_2 = I_2 - \frac{2}{3} I_1 - \frac{1}{3} I_0$.

$A^{(1)} = -2\left(\widetilde{C}_1 + 1\right) - 2.4 Q_1 + 0.8 Q_2 C'_2$
$A^{(2)} = -4 C'_1 \widetilde{C}_1 + 0.8 Q_1 C'_2$
$A^{(3)} = 0.8 + \frac{4}{3} b^2_{kk} C'_2$
$A^{(4)} = 1.2 + \left(0.4 + 2 b^2_{kk}\right) C'_2$
$A^{(5)} = \frac{26}{15} + 16 b^2_{kk} C_2 + \left(2 b^2_{kk} - \frac{14}{45}\right) C'_2$
$A^{(6)} = 0.8 - 2 C'_2$
$A^{(7)} = 0.8 + \frac{34}{15} C'_2$
$A^{(8)} = -1.6 + 3.2 C'_2$
$A^{(9)} = -48 C_2 - 8 C'_2$
$A^{(10)} = -4.8 C'_2$
$\widetilde{C}_1 = 2 C_1 \sqrt{F b^2_{kk}}$
$C_1 = 3.1$, $C'_1 = 1.2$, $C_2 = 0.55$ and $C'_2 = 0.6$.

The FLT model is summarised in Table V. The equation for turbulent dissipation ε based on the model by Merci and Dick[42] reads:

$$\frac{\partial \overline{\rho} \varepsilon}{\partial t} + \frac{\partial \overline{\rho} \widetilde{U}_j \varepsilon}{\partial x_j} = \mathscr{T}^{\varepsilon}_i + S_\varepsilon, \qquad (61)$$

where the source term S_ε combines the standard model:

$$S^{\mathrm{std}}_\varepsilon = \rho\,\omega \left(C_{\varepsilon 1} P_k - C_{\varepsilon 2} \varepsilon\right), \qquad (62)$$

together with the equation introduced by Shih *et al.*[43] in their realizable k-ε model, giving good results for free shear flows:

$$S^{\mathrm{Shih}}_\varepsilon = \rho \left(C'_{\varepsilon 1} S^* \varepsilon - C'_{\varepsilon 2} \frac{\varepsilon^2}{k + \sqrt{\nu \varepsilon}}\right), \qquad (63)$$

where $S^* = \omega\sqrt{2S_{ij}S_{ij}}$, and $\nu = \mu/\rho$ is the kinematic molecular viscosity. Following Merci and Dick[42], the model reads:

$$S_\varepsilon = \left(1 - f_{R_y}\right) S_\varepsilon^{\text{std}} + f_{R_y} S_\varepsilon^{\text{Shih}}, \quad (64)$$

where the blending function f_{R_y} goes from 0 to 1 between $R_y = 1000$ and $R_y = 2000$, with $R_y = (\sqrt{k}.y)/\nu$ and y the normal distance to the nearest solid boundary. We use the values $C_{\varepsilon 1} = 1.44$, $C_{\varepsilon 2} = C'_{\varepsilon 2} = 1.9$ and $C'_{\varepsilon 1} = \max\left\{0.43, \frac{S^*/\omega}{5+S^*/\omega}\right\}$. The diffusive term $\mathscr{T}_i^\varepsilon$ is modeled in a similar way as (19) and (27).

B. Swirling jet

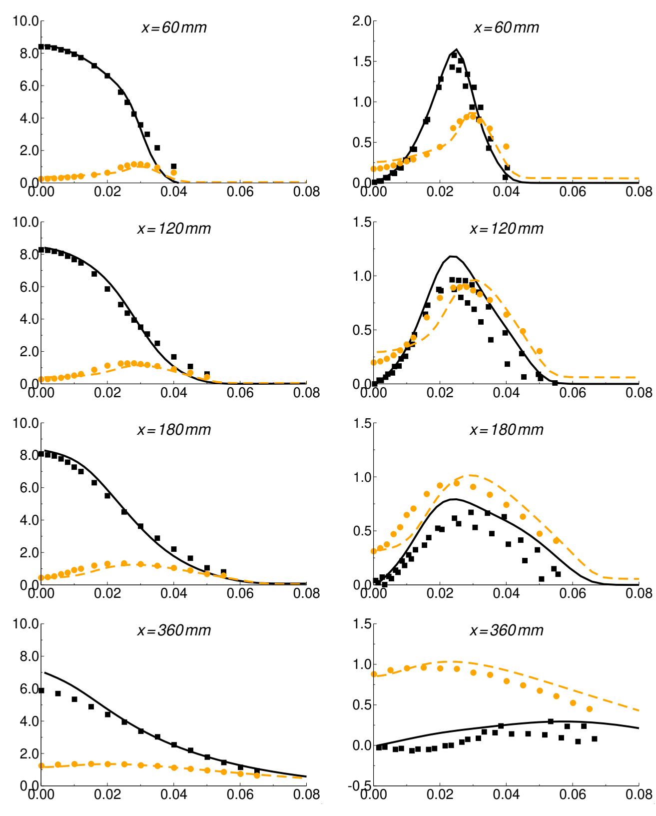

FIG. 1. Radial profiles of axial (left) and azimuthal (right) velocity from the turbulent swirling jet[44] at four axial locations. Symbols: experimental data. Lines: calculations. In black the mean velocities $\widetilde{U}$ and $\widetilde{W}$, and in orange the r.m.s. fluctuations $\sqrt{\widetilde{uu}}$ and $\sqrt{\widetilde{ww}}$.

The first case considered[44] is a swirling air jet issuing from a rotating pipe of radius $R = 0.03$m at a Reynolds number of 24000 and swirl number 0.5. The inlet profiles for the mean axial and azimuthal velocity components, $\widetilde{U}$ and $\widetilde{W}$, and for their r.m.s. fluctuations, $\sqrt{\widetilde{uu}}$ and $\sqrt{\widetilde{ww}}$ are set by interpolating the experimental data. The radial mean velocity $\widetilde{V}$ is set to zero at the inlet and its r.m.s. fluctuation is set as $\sqrt{\widetilde{vv}} = \sqrt{\widetilde{ww}}$. The fluctuating velocity correlations are set as $\widetilde{uv} = 0.5(r/R)\sqrt{\widetilde{uu}}\sqrt{\widetilde{vv}}$ and $\widetilde{uw} = -0.5(r/R)\sqrt{\widetilde{uu}}\sqrt{\widetilde{ww}}$, with r the radial distance, while supposing $\widetilde{vw} = 0$. Finally, the inlet profile for turbulent dissipation is set assuming $\varepsilon = -\widetilde{uv}(\partial U/\partial r)$, where the gradient $\partial U/\partial r$ is obtained from the profile $U(r) = U_c\,(1 - r/R)^{1/7}$, with U_c the experimental centerline velocity.

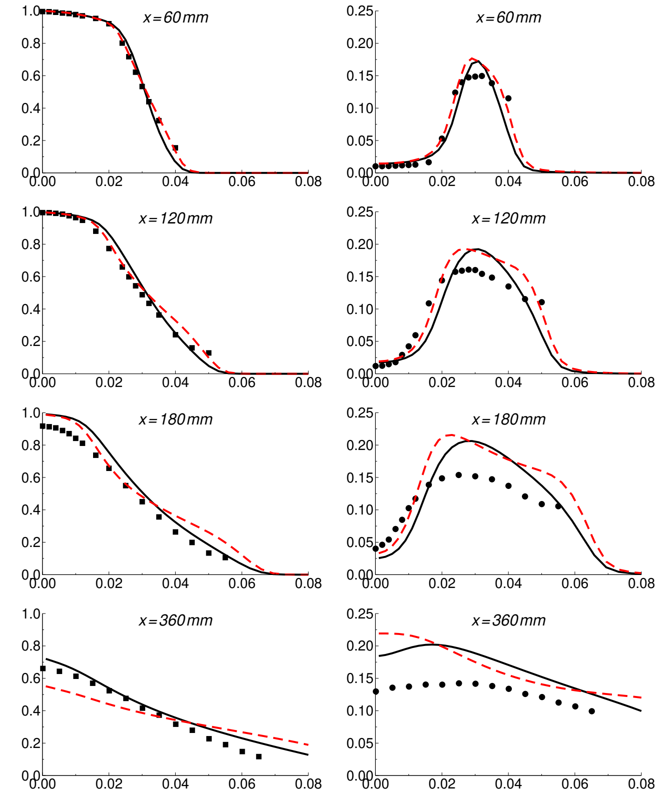

FIG. 2. Radial profiles of mean scalar $\widetilde{Z}$ (left) and its variance $\widetilde{Z''^2}$ (right) from the turbulent swirling jet[44] at four axial locations. Symbols: experimental data. Black lines: variable C_0 formulation. Red dashed lines: constant C_0 formulation ($C_0 = 2.1$). In both cases, $C_\phi^* = 0$.

The 2D-axisymmetric domain is 1.2m long in the axial direction and 0.6m wide in the radial direction, and is discretized using a cartesian grid consisting of 105×105 cells stretched in both directions.

Figure 1 shows that good results are obtained for the flow field, demonstrating that the FLT Reynolds-stress model combined with Merci and Dick turbulent dissipation is able to correctly model both the mean and fluctuating velocity.

Figure 2 then gives an interesting comparison for the purpose of this paper. The results for mean scalar and scalar variance are shown when using either the variable C_0 GLM implying (40), either the constant C_0 GLM implying (25), in both cases supposing $C_\phi^* = 0$. We can observe discrepancies resulting from the different scalar-flux models and, in particular at the last axial location ($x = 360$mm), the constant C_0 GLM results leads to worse results.

C. Bluff-body jet with recirculation

The second case is a turbulent C_2H_4 jet issuing from the middle of a cylinder surrounded by an air coflow, implying a recirculation above the cylinder. This is a non-reacting jet corresponding to the series of Sydney bluff-body stabilized flames[45,46] which are target flames of the International Workshop on Measurement and Computation of Turbulent Flames[47]. The numerical settings are the same as previous calculations for reacting cases[22], and the inlet boundary conditions are slightly revised compared to previous calculations of the same non-reacting flow[35]. In the following, $R_j = 0.18$cm refers to the central pipe radius, and D_b and R_b refer respectively to the diameter and radius of the bluff-body: $D_b = 5$cm and $R_b = 2.5$cm.

The inlet conditions in the turbulent jet are set by specifying a profile for mean axial velocity $U(r) = |U|\,(1.01 - r/R_j)^{1/6}$ and assuming that turbulent dissipation satisfies $\varepsilon = -\widetilde{uv}(\partial U/\partial r)$, where $|U|$ is chosen to make sure that the correct jet bulk velocity $U_{\text{jet}} = 61$m/s is imposed (i.e. correct mass flux). The r.m.s. velocity fluctuations are set to be equal in axial, radial and azimuthal directions ($\sqrt{\widetilde{uu}}$, $\sqrt{\widetilde{vv}}$ and $\sqrt{\widetilde{ww}}$, respectively). They are obtained from the following fit of the experimental data: $\sqrt{\widetilde{uu}} = \sqrt{2/3}U_{\text{jet}}0.1\,(1.1 - r/R_j)^{-1/6}$. The turbulent shear stress is defined as $\widetilde{uv} = 0.5(r/R_j)\sqrt{\widetilde{uu}}\sqrt{\widetilde{vv}}$.

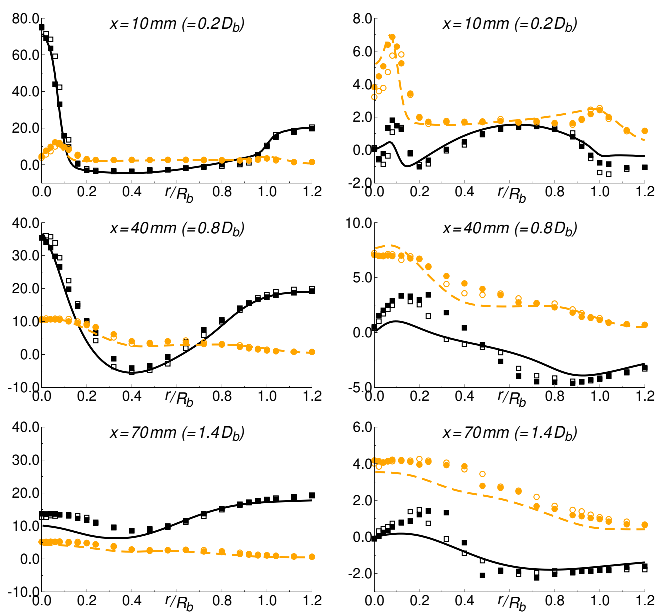

FIG. 3. Radial profiles of axial (left) and radial (right) velocity from Sydney turbulent bluff-body jet[45] at three axial locations. Symbols: two sets of experimental data. Lines: calculations. In black the mean velocities $\widetilde{U}$ and $\widetilde{V}$, and in orange the r.m.s. fluctuations $\sqrt{\widetilde{uu}}$ and $\sqrt{\widetilde{vv}}$.

In the coflow, profiles are specified between $r = R_b$ and $r = R_b + \delta$, supposing a boundary layer thickness $\delta = 0.5$cm. Fits of the experimental data are applied using the bulk coflow velocity $U_{\text{cof}} = 20$m/s. For the mean axial velocity: $\widetilde{U} = U_{\text{cof}}\,[(r - R_b)/\delta]^{1/10}$. For velocity fluctuations: $\sqrt{\widetilde{uu}} = 0.0281U_{\text{cof}}\,[(R_b + 0.2\delta - r)/\delta]^{-1/2}$ if $r < R_b + 0.2\delta$ and $\sqrt{\widetilde{uu}} = 0.0281U_{\text{cof}}\,[(r - R_b)/\delta]^{-1/2}$ otherwise. We use $\widetilde{uv} = 0.5\,[(r - R_b)/\delta]\,\sqrt{\widetilde{uu}}\sqrt{\widetilde{vv}}$ if $r < R_b + \delta$ and $\widetilde{uv} = 0$ otherwise, and again $\varepsilon = -\widetilde{uv}(\partial U/\partial r)$. Note that the calculations are particularly sensitive to the specification of the turbulent shear stress $\widetilde{uv}$ in the coflow.

Figure 3 shows that, with the specified inlet profiles, the mean turbulent flow is again very well predicted using the FLT Reynolds-stress model together with Merci and Dick turbulent dissipation.

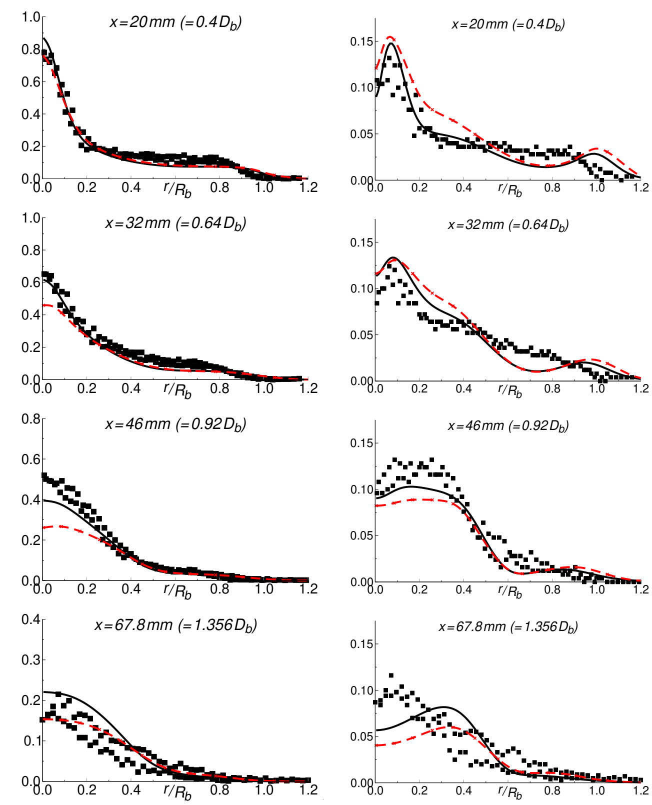

FIG. 4. Radial profiles of mean scalar $\widetilde{Z}$ (left) and its variance $\widetilde{Z''^2}$ (right) from Sydney turbulent bluff-body jet[45] at four axial locations. Symbols: experimental data. Black lines: variable C_0 formulation. Red dashed lines: constant C_0 formulation ($C_0 = 2.1$). In both cases, $C^*_\phi = 0$.

For this challenging recirculating flow, we are again interested in comparing the variable C_0 GLM to the constant C_0 GLM, implying different turbulent scalar-flux models. Figure 4 shows that the correct Monin's term implied by the variable C_0 GLM ensures a correct profile for $\widetilde{Z}$, while the constant C_0 GLM leads to an underprediction of the centerline values. Moreover, the shape of scalar variance profiles in the recirculation zone is better predicted by the variable C_0 GLM implied model.

D. Bluff-body particle-laden jet with recirculation

In order to validate the proposed variable C_0 two-phase GLM for particle dispersion, we consider the 'Hercule' confined polydispersed two-phase flow downstream of a bluff-body[48,49]. The 'Hercule' configuration, is representative of pulverized coal combustion devices where primary air and coal are injected in the central pipe and where secondary air is injected as a coflow around the bluff-body. Note however that this experimental set-up has no swirling motion. In this case, the coflow is rather an 'annular flow' since this is a confined configuration, with a central pipe of radius $R_j = 1$cm, a bluff-body of diameter $R_b = 7.5$cm and a lateral wall at $R_2 = 15$cm.

The air is injected at ambient temperature at rather low velocities (3.4m/s in the jet and 6m/s in the coflow), implying a rather low Reynolds number of about 4500 at the exit of the central pipe. A typical bluff-body flow with recirculation behind the bluff-body is created. The solid particles injected in the central pipe are glass particles (density $\rho_p =$ 2450 kg/m^3), with diameter distribution between $D_p = 20\mu$m and $D_p = 110\mu$m, around the mean value $D_p = 60\mu$m. The mass loading of 22% at the inlet is high enough to moderately affect the mean gas flow velocity and Reynolds stresses, however, we will not consider two-way coupling effects here. This test case is interesting for validation of dispersion models since the particles interact with negative axial velocities in the recirculation zone.

The 2D axisymmetric computational domain starts at the injector exit plane (at bluff-body surface). It is 0.45m long, and extends to the outer wall in the radial direction ($R_2 =$ 0.15m). In the axial direction, the cartesian grid is stretched and contains 120 cells. In the radial direction, the mesh is uniform in the central pipe and on the bluff-body surface (8 cells in the pipe and 52 cells on the bluff body), and it is stretched in the coflow (40 cells). Free-slip conditions are applied on the bluff-body surface and on the lateral wall.

The inlet conditions are specified in a similar way as the previous bluff-body jet. In the central pipe we impose the experimental continuous phase mass flux with the mean axial velocity profile $\widetilde{U} = |U|\left[1.01 - r/R_j\right]^{1/6}$. The profiles from axial and radial Reynolds stresses (resp. $\widetilde{uu}$ and $\widetilde{vv}$) are directly interpolated from experimental data, and we suppose $\widetilde{ww} = \widetilde{vv}$. We again specify the turbulent shear stress profile as $\widetilde{uv} = 0.5(r/R_j)\sqrt{\widetilde{uu}}\sqrt{\widetilde{vv}}$ and the turbulent dissipation as $\varepsilon = -\widetilde{uv}(\partial U/\partial r)$. In the annular flow, we fit the experimental profiles using the formulas given in Table VI. The azimuthal Reynolds stresses are set to $\widetilde{ww} = \widetilde{vv}$. Turbulent dissipation is set as $\varepsilon = C_\mu^{3/4} k^{3/2}/(\kappa\delta)$, with $C_\mu = 0.09$, $\kappa = 0.4$ and the half-width of the annular distance $\delta = 3.75$cm.

For the dispersed phase, ten droplet size classes are considered, with diameters 10, 20, 30, 40, 50, 60, 70, 80, 90 and 100μm. The same velocity profiles are specified for all droplet size classes: equal to the continuous phase velocity profiles in the fuel pipe (mean axial velocity and Reynolds stresses). The experimental mass flux is specified for each size class. One more class is considered for validation: tracer particles of diameter 3μm.

TABLE VI. Fits of experimental inlet profiles in the annular flow, with $U_{\text{cof}} = 6$m/s

$\widetilde{U}$	$= U_{\text{cof}}\left[\frac{r-0.075}{0.1-0.075}\right]^{1/10}$	$0.075 \le r \le 0.1$
	$= U_{\text{cof}}\left[\frac{0.15-r}{0.15-0.1}\right]^{1/6}$	$0.1 \le r \le 0.15$
$\widetilde{V}$	$= 961.54\,(r-0.088)^2 + 2.5\,(r-0.14)$	$0.075 \le r \le 0.88$
	$= 2.5\,(r-0.14)$	$0.88 \le r \le 0.14$
	$= 0$	$0.14 \le r \le 0.15$
$\sqrt{\widetilde{uu}}$	$= 720\,(r-0.1)^2 + 0.2$	$0.075 \le r \le 0.1$
	$= 200\,(r-0.1)^2 + 0.2$	$0.1 \le r \le 0.15$
$\sqrt{\widetilde{vv}}$	$= 200\,(r-0.1)^2 + 0.173$	$0.075 \le r \le 0.1$
	$= 80\,(r-0.1)^2 + 0.173$	$0.1 \le r \le 0.15$
$\widetilde{uv}$	$= -80\,(r-0.1)^2 + 1.2\,(r-0.1)$	$0.075 \le r \le 0.1$
	$= 1.2\,(r-0.1)$	$0.1 \le r \le 0.14$
	$= 4.8\,(0.15-r)$	$0.14 \le r \le 0.15$

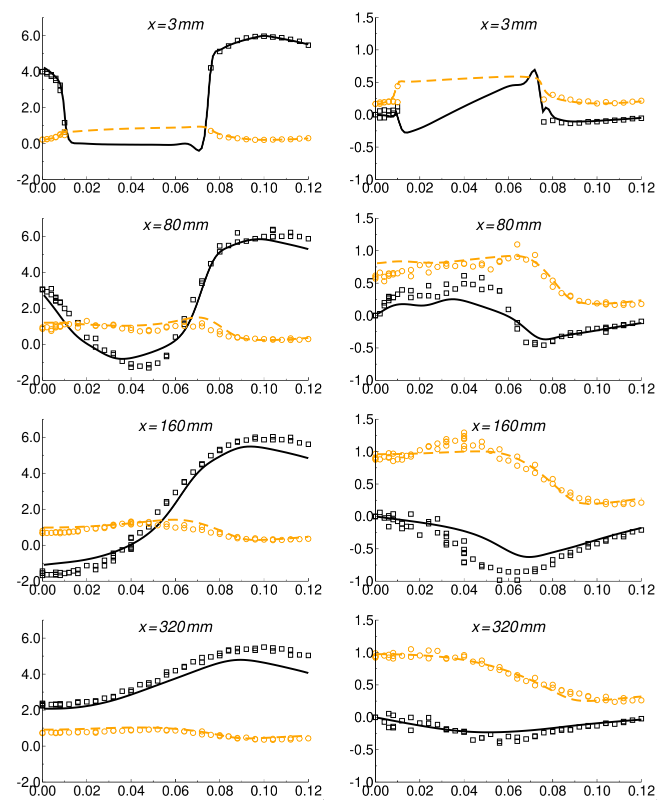

FIG. 5. Radial profiles of axial (left) and radial (right) velocity of the continuous phase of 'Hercule' confined polydispersed two-phase bluff-body flow[48], at four axial locations. Symbols: experimental data. Lines: calculations. In black the mean velocities $\widetilde{U}$ and $\widetilde{V}$, and in orange the r.m.s. fluctuations $\sqrt{\widetilde{uu}}$ and $\sqrt{\widetilde{vv}}$.

As for the other cases, Figure 5 shows that the turbulent flow field is correctly modeled by the FLT Reynolds-stress model. Note that in this confined case, we simply used the standard modeled equation (62) for ε.

Figures 6, 7 and 8 show the particle mean velocities and

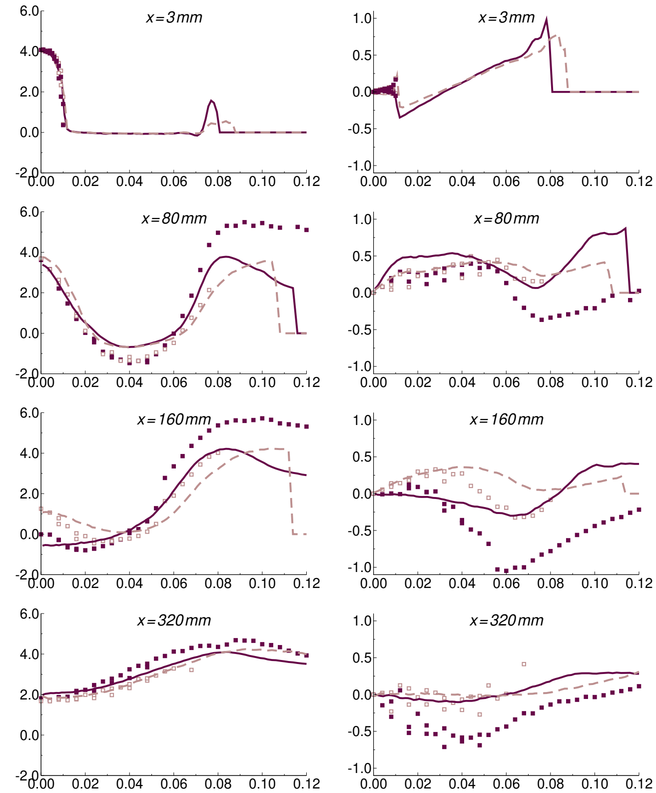

FIG. 6. Hercule's dispersed phase mean velocity: axial $\langle U\rangle_{\mathrm{p}}$ (left) and radial $\langle V\rangle_{\mathrm{p}}$ (right). Two size classes: 20μm (filled symbols and continuous lines) and 90μm (opened symbols and dashed lines). Symbols: experimental data. Lines: variable C_0-GLM calculations.

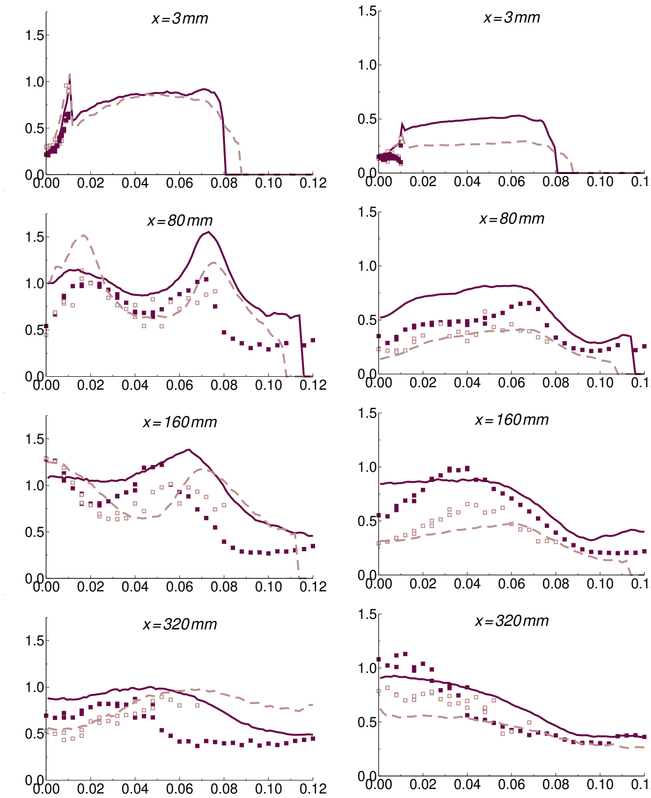

FIG. 7. Hercule's dispersed phase r.m.s. velocity fluctuations: axial $\sqrt{\langle uu\rangle_{\mathrm{p}}}$ (left) and radial $\sqrt{\langle vv\rangle_{\mathrm{p}}}$ (right), for two size classes (see Figure 6).

velocity correlations obtained with the variable C_0 two-phase GLM, for two different particle size classes: the smallest measured particles of diameter 20μm and one of the largest size class of diameter 90μm. We can observe that the results are in good agreement with the experimental data and that the model correctly captures the behaviour of the different size classes.

The results (both for the fluid and the particles) are similar to the results obtained by Minier *et al.*[28]. However, the current mean fluid velocity results are in better agreement with experimental data. For this not too high Reynolds number test case, this difference in the results could probably be mostly due to the different specification of the inlet boundary profiles, rather than to the use of different Reynolds-stress models. It is difficult to directly compare the results for the dispersed phase since we compare here the results for different size classes while Minier *et al*. considered global averages over all size classes. Note that it is hard to make a comparison of the modeling of tracer particles since they considered mass weighted averages, where the contribution of the smallest particles is reduced.

We can finally compare in Figure 9 the mean volume fraction α of the smallest particles considered (tracer particles of diameter 3μm), obtained from (49), to a mean passive scalar $\widetilde{Z}$ transported in the continuous phase. Note that both properties are not strictly equivalent. The modeling of the triple

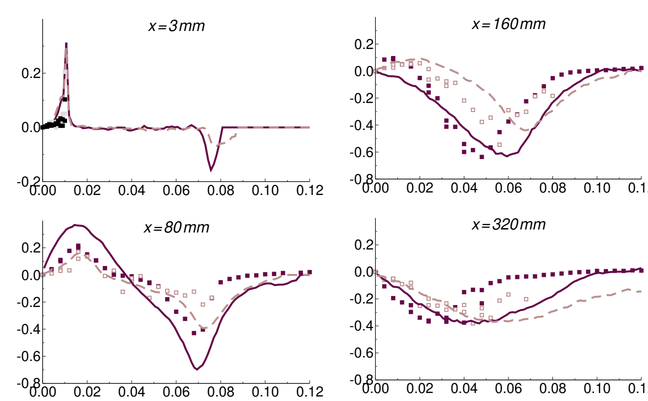

FIG. 8. Hercule's dispersed phase velocity correlation $\langle uv\rangle_{\mathrm{p}}$ for two size classes (see Figure 6).

correlations $\mathscr{T}_i^Z$ is not the same, since the approximation (27) is used when solving $\widetilde{Z}$. Still, we see a good correspondence between both.

As in the previous cases, we can then observe the effect of the choice of the GLM formulation on mean scalar mixing ($\widetilde{Z}$), and tracer particle dispersion (α). The results are consistent with the previous bluff-body jet where the constant C_0 GLM implies lower centerlines values. We can clearly see the effect

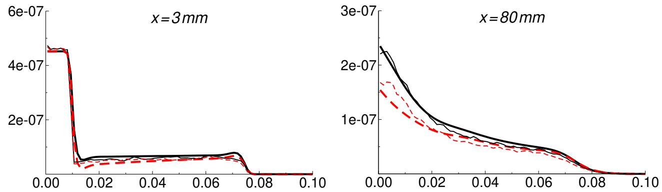

FIG. 9. Volume fraction from 3μm tracer particles (thin lines) compared to passive scalar (thick lines). Black lines: variable C_0 formulation. Red dashed lines: two-phase GLM based on constant C_0 formulation ($C_0 = 2.1$). In both cases, $C_\phi^* = 0$.

of the proposed variable C_0 two-phase GLM which imposes the Monin's return-to-isotropy term in the scalar-flux modeling. The constant C_0 version of the proposed two-phase GLM cannot represent the effects of the Monin term and the proposed non-constant C_0 version is needed to correctly predict dispersion of the smallest particles in polydispersed sprays.

VI. CONCLUSIONS

In the context of joint velocity-scalar PDF modeling, two general Generalized Langevin Model (GLM) formulations were recalled and detailed, where the coefficients can be specified in order to imply a chosen Reynolds-stress model: a GLM formulation using a non-constant C_0 diffusion coefficient and the standard constant C_0 formulation. The implied scalar-flux second-moment closure was derived in both cases. It was recalled that the standard formulation generally does not imply the correct Monin's return-to-isotropy term, while the proposed non-constant C_0 formulation does (even when a contribution from the micro-mixing model needs to be taken into account).

It was explained that the deficiency of the constant C_0 GLM has to be considered as well in Lagrangian modeling of dispersed two-phase flows based on a two-phase Simplified Langevin Model. In this case, the modeling of tracer particle dispersion corresponds to the modeling of a passive scalar. As an extension of the non-constant C_0 GLM, a new two-phase velocity GLM was proposed.

In order to deal with complex turbulent jets including swirl and recirculation zones, the cubic Reynolds-stress model of Fu, Launder and Tselepidakis is used, together with Merci and Dick turbulent dissipation model. Results are presented for two single-phase turbulent jets, a swirling jet and a bluff-body jet with recirculation, and for a polydispersed particle laden jet with recirculation. In all cases, the results for the flow field are in very good agreement with the experimental data.

Scalar mixing or particle dispersion when using either the standard or proposed formulations of the GLM are then compared for all three cases. In both single-phase jets, where experimental data is available, we verified that the proposed non-constant C_0 formulation indeed allows to better model scalar mixing. This validates the approach of imposing a modeling of the return-to-isotropy term in the implied scalar-flux model, consistent with Monin's standard constant value. The same behavior is observed for tracer particle dispersion, indicating that the proposed two-phase GLM should be preferred for dispersed two-phase flow modeling.

ACKNOWLEDGMENTS

Part of this work is supported at Ciemat by the project #PID2019-108592RB-C42/AEI/10.13039/50110 0 011033.

DATA AVAILABILITY

The data that support the findings of this study are available from the corresponding author upon reasonable request.

[1]C. Dopazo and E.E. O'Brien. An approach to the autoignition of a turbulent mixture. *Acta Astronautica*, 1:1239-1266, 1974.
[2]S.B. Pope. PDF methods for turbulent reactive flows. *Progress in Energy and Combustion Science*, 11:119-192, 1985.
[3]D.C. Haworth and S.B. Pope. A generalized Langevin model for turbulent flows. *Physics of Fluids*, 29:387-405, 1986.
[4]S.B. Pope. On the relationship between stochastic Lagrangian models of turbulence and second-moment closures. *Physics of Fluids*, 6:973-985, 1994.
[5]P.A. Durbin and C.G. Speziale. Realizability of second-moment closure via stochastic analysis *Journal of Fluid Mechanics*, 280:395-407, 1994.
[6]H.A. Wouters, T.W.J. Peeters and D. Roekaerts. On the existence of a Generalized Langevin model representation for second-moment closures. *Physics of Fluids*, 8:1702-1704, 1996.
[7]B. Naud, B. Merci and D. Roekaerts. Generalised Langevin Model in correspondence with a chosen standard scalar-flux second-moment closure. *Flow, Turbulence and Combustion*, 85:363-382, 2010.
[8]B.L. Sawford. Reynolds number effects in Lagrangian stochastic models of turbulent dispersion. *Physics of Fluids A*, 3:1577-1586, 1991.
[9]S.B. Pope. Lagrangian PDF methods for turbulent flows. *Annu. Rev. Fluid Mech.*, 26:23-63, 1994.
[10]M.S. Anand and S.B. Pope. Diffusion behind a line source in grid turbulence. In *Turbulent Shear Flows 4 (Edited by L.J.S. Bradbury, F. Durst, B.E. Launder, F.W. Schmidt and J.H. Whitelaw)*, p. 46, Springer-Verlag, Berlin, 1985.
[11]S. Viswanathan and S.B. Pope. Turbulent dispersion from line sources in grid turbulence. *Physics of Fluids*, 20:1-25, 2008.
[12]A.S. Monin. On the symmetry properties of turbulence in the surface layer of air. *IZV Atm. Oceanic, Phys.*, 1:45-54, 1965.
[13]J.-P. Minier and E. Peirano. The pdf appraoch to turbulent polydispersed two-phase flow. *Physics Reports*, 352:1-214, 2001.
[14]O. Simonin, E. Deutsch and J.-P. Minier. Eulerian prediction of the fluid/particle correlated motion in turbulent two-phase flows. *Applied Scientific Research*, 51:275-283, 1993.
[15]J.-P. Minier, S. Chibbaro and S.B. Pope. Guidelines for the formulation of Lagrangian stochastic models for particle simulations of single-phase and dispersed two-phase turbulent flows. *Physics of Fluids*, 26, 113303, 2014.
[16]A. Innocenti, R.O. Fox, M.V. Salvetti and S. Chibbaro. A Lagrangian probability-density-function model for collisional turbulent fluid-particle flows. *J. Fluid Mech.*, 862:449-489, 2019.
[17]P. Durbin and Y. Shabany. Toward consistent formulation of Reynolds stress and scalar flux closures. *Fluid Dynamics Research*, 20:115-125, 1997.
[18]S. Fu, B.E. Launder, D. Tselepidakis. Acccommodating the effects of high strain rates in modelling the pressure-Strain correlation. Technical report TFD/87/5, UMIST, March 1987.
[19]S.B. Pope. *Turbulent Flows*, Cambridge University Press, 2000.
[20]M. Muradoglu, S.B. Pope and D.A. Caughey. The hybrid method for the PDF equations of turbulent reactive flows: consistency conditions and correction algorithm. *Journal of Computational Physics*, 172:841-878, 2001.

[21] E. Peirano, S. Chibbaro, J. Pozorski and J.-P. Minier. Mean-field/PDF numerical approach for polydispersed turbulent two-phase flows *Progress in Energy and Combustion Science*, 32:315-371, 2006.

[22] B. Naud, C. Jiménez and D. Roekaerts. A consistent hybrid PDF method: implementation details and application to the simulation of a bluff-body stabilised flame. *Progress in Computational Fluid Dynamics*, 6:146-157, 2006.

[23] R.O. Fox. On velocity-conditioned scalar mixing in homogeneous turbulence. *Physics of Fluids*, 8:2678-2691, 1996.

[24] S.B. Pope. The vanishing effect of molecular diffusivity on turbulent dispersion: implications for turbulent mixing and the scalar flux. *Journal of Fluid Mechanics*, 359:299-312, 1998.

[25] J. Villermaux and J.C. Devillon. In *Proc. Second Int. Symp. On Chemical Reaction Engineering*, New York, Elsevier, 1972.

[26] B.E. Launder. Heat and mass transport. In *Turbulence, (Edited by P. Bradshaw), Topics in Applied Physics*, 12:231-287, Springer, 1978.

[27] J.L. Lumley. Computational modeling of turbulent flows. *Advances in Applied Mechanics*, 18:123-176, 1978.

[28] J.-P. Minier, E. Peirano and S. Chibbaro. PDF model based on Langevin equation for polydispersed two-phase flows applied to a bluff-body gas-solid flow. *Physics of Fluids*, 16:2419-2431, 2004.

[29] O. Simonin. Statistical and continuum modeling of turbulent reactive flows – part I. Lecture series 2000-06 of the von Karman Institute: Theoretical and Experimental Modelling of Particulate Flow, 3-7 April 2000.

[30] B. Naud. PDF modeling of turbulent sprays and flames using a particle stochastic approach. Ph.D. thesis, Delft University of Technology. Downloadable from http://www.darenet.nl/promiseofscience (2003)

[31] M. Stöllinger, B. Naud, D. Roekaerts, N. Beishuizen and S. Heinz. PDF modeling and simulations of pulverized coal combustion – Part 1: Theory and modeling *Combustion and Flame*, 160:384-395, 2013.

[32] R. Gatignol. The Faxén formulae for a rigid particle in an unsteady non-uniform Stokes flow. *J. Méc. Théor. Appl*, 1:143-160, 1983.

[33] M.R. Maxey, J.J. Riley. Equation of motion for a small rigid sphere in a nonuniform flow. *Physics of Fluids*, 26:883-889, 1983.

[34] G.T. Csanady. Turbulent diffusion of heavy particles in the atmosphere. *Journal of the Atmospheric Sciences*, 20:201-208, 1963.

[35] G. Li, B. Naud and D. Roekaerts, "Numerical Investigation of a Bluff-Body Stabilised Nonpremixed Flame with Differential Reynolds-Stress Models," *Flow, Turbulence and Combustion* **70**, 211-240 (2003).

[36] N.A. Beishuizen, B. Naud and D. Roekaerts, "Evaluation of a modified Reynolds stress model for turbulent dispersed two-phase flows including two-way coupling," *Flow, Turbulence and Combustion* **79**, 321-341 (2007).

[37] B. Merci, B. Naud, D. Roekaerts and U. Maas, "Joint scalar versus joint velocity-scalar PDF simulations of bluff-body stabilized flames with REDIM," *Flow, Turbulence and Combustion* **82**, 185-209 (2009).

[38] R. De Meester, B. Naud, U. Maas and B. Merci, "Transported scalar PDF calculations of a swirling bluff body flame ('SM1') with a reaction diffusion manifold," *Combustion and Flame* **159**, 2415-2429 (2012).

[39] M. Stöllinger, B. Naud, D. Roekaerts, N. Beishuizen and S. Heinz, "PDF modeling and simulations of pulverized coal combustion – Part 2: Application," *Combustion and Flame* **160**, 396-410 (2013).

[40] B. Naud, R. Novella, J.M. Pastor and J.F. Winklinger, "RANS modelling of a lifted H_2/N_2 flame using an unsteady flamelet progress variable approach with presumed PDF," *Combustion and Flame* **162**, 893-906 (2015).

[41] L. Ma, B. Naud and D. Roekaerts, "Transported PDF modeling of ethanol spray in hot-diluted coflow flame," *Flow, Turbulence and Combustion* **96**, 811-820 (2016).

[42] B. Merci, E. Dick. Predictive capabilities of an improved cubic k-ε model for inert steady flows. *Flow, Turbulence and Combustion*, 68:335-358, 2002.

[43] T. Shih, W.W. Liou, A. Shabbir, Z. Yang and J. Zhu A new k-ε eddy viscosity model for high Reynolds number turbulent flows *Computers Fluids*, 24(3):227-238, 1995.

[44] R. Örlü. Experimental study of passive scalar mixing in swirling jet flows. Technical report, from Royal Institute of Technology, KTH Mechanics, SE-100 44 Stockholm, Sweden, September 2006.

[45] B.B. Dally and A.R. Masri. Flow and mixing fields of turbulent bluff-body jets and flames. *Combustion Theory and Modelling*, 2:193-219, 1998.

[46] B.B. Dally, A.R. Masri, R.S. Barlow and G.J. Fiechtner. Instantaneous and mean compositional structure of bluff-body stabilized nonpremixed flames. *Combustion and Flame*, 114:119-148, 1998.

[47] R.S. Barlow. International Workshop on Measurement and Computation of Turbulent Nonpremixed Flames. http://www.ca.sandia.gov/TNF

[48] T. Ishima, J. Borée, P. Fanouillère, and I. Flour. Presentation of a two phase flow data base obtained on the flow loop Hercule. In *9th Workshop on Two-phase Flow Predictions*, Martin-Luther-Universität, Halle-Wittenburg, Germany, 1999. http://www-mvt.iw.uni-halle.de/testfaelle/hercule-_2-phasenstroemung/

[49] J. Borée, T. Ishima and I. Flour. The effect of mass loading and inter-particle collisions on the development of the polydispersed two-phase flow downstream of a confined bluff body. *Journal of Fluid Mechanics*, 443:129-165, 2001.